communications chemistry

A Nature Portfolio journal

Article

https://doi.org/10.1038/s42004-025-01534-x

A rare peptide scaffold in kineomicins, the glycopeptide antibiotics produced by *Actinokineospora auranticolor* DSM 44650

Oleksandr Yushchuk[1,6], Francesca Berini[2,6], Lei Zhong[3,6], Christian Rückert-Reed[4,5], Elena Bernasconi[2,3], Letizia Bartolone[2], Tobias Busche[4], Jörn Kalinowski[4], Roderich D. Süssmuth[3,7] ✉ & Flavia Marinelli[2,7] ✉

Discovery of novel antibiotics is crucial to counteract bacterial resistance spread. Aiming to expand the available arsenal of last-resort glycopeptide antibiotics (GPAs), we mined the actinobacterial genomes of *Pseudonocardiales*. We thus identified a biosynthetic gene cluster (BGC) encoding for a GPA with a novel peptide scaffold, not fitting into the existing classification of GPA types. By cultivating the producer strain, *Actinokineospora auranticolor* DSM 44650, an antibiotic complex—named kineomicins (Kmc)—was identified and characterized by microbiological assays, LC-MS, and MS/MS analyses. A comprehensive model for Kmc biosynthesis was then proposed by a thorough investigation of kineomicin BGC (*knm*). The structure of the main complex congener (KmcB), resolved by NMR spectroscopy, proved to be unique. Finally, the remarkably high antibiotic production rate, up to >1 g L^{-1} Kmc in benchtop bioreactor, indicated *A. auranticolor* as a natural GPA overproducer, holding promise as a potential host for heterologous expression of GPA BGCs.

Glycopeptide antibiotics (GPAs) constitute a diverse and still expanding group of naturally occurring non-ribosomally synthesized peptide antibiotics[1–4]. These antibiotics are produced by Gram-positive bacteria found in soil, belonging to actinobacterial orders such as *Kitasatosporales*, *Micromonosporales*, *Streptosporangiales*, and *Pseudonocardiales*[1]. GPAs have proven clinically effective in treating infections caused by multidrug-resistant (MDR) Gram-positive pathogens in both children and adults[5,6]. Notable examples include vancomycin and teicoplanin, which are natural GPAs in clinical use, derived from *Amycolatopsis* spp. (order *Pseudonocardiales*)[7,8] and *Actinoplanes teichomyceticus* ATCC 31121[9] (order *Micromonosporales*), respectively. Additionally, semi-synthetic GPAs such as dalbavancin, oritavancin, and telavancin[10] have been developed from A40926 (produced by *Nonomuraea gerenzanensis* ATCC 39727[11], order *Streptosporangiales*), chloroeremomycin (*Kibdelosporangium aridum* A82846[12], order *Pseudonocardiales*), and vancomycin, respectively, and more recently approved for clinical application.

The story of this antibiotic class began with the discovery of vancomycin, ristocetin, and actinoidin in the 1950s[13–15]. The clinical success of vancomycin brought GPAs into the spotlight, leading to various bioactivity-guided screening programs of environmental isolates of actinomycetes[1]. During the 1980s, numerous and structurally diverse natural sourced GPAs were isolated, and teicoplanin[16] entered the clinics. It was meantime discovered that GPAs bind to the D-alanyl-D-alanine (D-Ala-D-Ala) termini of nascent peptidoglycan, hindering cell wall biosynthesis in Gram-positive bacteria[17]. The common feature of these GPAs was recognized as a sidechain cross-linked peptide core consisting of seven amino acids, whose structural variations led to the first (and still valid) classification (dated 1999) into five structural types[1]. GPAs of Types I-IV are considered *glyco*peptides *sensu stricto*, and they are also named dalbaheptides[18], whereas Type V comprises non-glycosylated antibiotics[1]. Type I compounds (e.g., vancomycin, balhimycin, chloroeremomycin[19]) contain aromatic amino acids in positions AA2, 4-7, and aliphatic amino acids in positions AA1 and AA3

[1]Department of Genetics and Biotechnology, Ivan Franko National University of Lviv, Hrushevskoho St. 4, 79005 Lviv, Ukraine. [2]Department of Biotechnology and Life Sciences, University of Insubria, via J. H. Dunant 3, 21100 Varese, Italy. [3]Institute of Chemistry, Technische Universität Berlin, Strasse des 17. Juni 124, 10623 Berlin, Germany. [4]Technology Platform Genomics, CeBiTec, Bielefeld University, Sequenz 1, 33615 Bielefeld, Germany. [5]Medical School OWL, Bielefeld University, Sequenz 1, 33615 Bielefeld, Germany. [6]These authors contributed equally: Oleksandr Yushchuk, Francesca Berini, Lei Zhong. [7]These authors jointly supervised this work: Roderich D. Süssmuth, Flavia Marinelli. ✉e-mail: suessmuth@chem.tu-berlin.de; flavia.marinelli@uninsubria.it

(Supplementary Fig. 1). Cross-linking occurs between aryl rings at AA7 (denoted as *A*) and AA5 (*B*), AA6 (*C*) and AA4 (*D*), and AA4 and AA2 (*E*) in Type I GPAs (Supplementary Fig. 1). In Type II GPAs, all amino acids are aromatic, with aryl rings introduced at AA3 (*F*) and AA1 (*G*), although *F* and *G* are not cross-linked (e.g., avoparcin, keratinimicin[20]) (Supplementary Fig. 1). Type III GPAs display cross-linking between aromatic AA1 and AA3 (e.g., ristocetin[21]) (Supplementary Fig. 1). Type IV GPAs (e.g., teicoplanin, A40926[22]) differ from Type III by carrying an aliphatic side chain (Supplementary Fig. 1). Type V compounds (e.g., complestatin, kistamicin[23]) feature a tryptophan residue in position AA2 and display more variable cross-linking patterns (Supplementary Fig. 1).

At the beginning of the 21st century, the development of DNA sequencing technologies enabled the identification of large biosynthetic gene clusters (BGCs) that encode GPA biosynthesis as in the case of chloroeremomycin[24], complestatin[25], teicoplanin[26], and A40926[27]. An extensive investigation of the roles of different genes and enzymes in GPA biosynthesis followed and led to the understanding of its main steps, *i.e.*, the aglycone synthesis[28–30], the biosynthesis of non-proteinogenic amino acids[31–33] and aminosugars[34], as well as of the tailoring reactions involved in GPA diversification[35–37]. Shortly after, the onset of the "genomic" era allowed for the complete sequencing of the genomes of GPA producers or of new isolates, facilitating the identification of novel BGCs and promoting the discovery of structurally novel compounds[8,21,38,39]. Actually, we are in a "postgenomic" era, in which phylogenomic tools are being applied to identify novel GPA BGCs and investigate their evolution[40–44]. Novel gene-engineering tools are being utilized to design heterologous hosts for GPA production and manipulate native producer strains[40,45,46], and multi-disciplinary approaches are being employed to unravel the intricate details of non-ribosomal peptide synthetase (NRPS) structure and functions[23,47–49], with the essential support of advanced analytical chemistry techniques[20]. In the light of this progress, the 1999-dated back classification of GPAs based on their chemical structure has been recently widened including diverse novel members of Type V GPAs discovered in *Streptomyces* spp.[40,42,43] (order *Kitasatosporales*), whose peptide core might extend up to 10 amino acids, exhibiting variable cross-linking patterns[40,42,43]. Furthermore, these Type V GPAs inhibit the growth of Gram-positive bacteria by a novel mode of action, *i.e.*, impeding cell wall turnover through the inhibition of autolysins[42,43]. A recent extensive evolutionary reconstruction has thus recommended categorizing Type V antibiotics as a novel class of glycopeptide-related peptides (GRPs), suggesting that the term GPA should be limited to Type I-IV dalbaheptides[18,50].

In this context, our discovery strategy was searching for novel GPAs with unconventional peptide scaffolds through comparative genomic analysis, exploiting such actinobacterial orders as *Micromonosporales*, *Streptosporangiales*, and *Pseudonocardiales* that are less represented (in terms of number of isolates and of genome sequences available) than the well-studied streptomycetes (order *Kitasatosporales*)[51]. In this study, we focused on *Pseudonocardiales*, that were demonstrated to be a quite prolific source of GPA BGCs and corresponding compounds[40,41,52]. *Pseudonocardiales* produce: Type I GPAs as vancomycin and chloroeremomycin (*vide supra*), as well as the model GPA balhimycin (this last produced by *Amycolatopsis balhimycina* DSM 5908)[35]; Type II GPAs, such as avoparcin (from *Amycolatopsis coloradensis* DSM 44225)[53], and the recently discovered keratinimicin (from *Amycolatopsis keratiniphila* NRRL B-24117)[20]; Type III GPAs (with multiple *Amycolatopsis* strains described as producers of ristocetin)[21,39,54]; and Type IV GPAs (e.g., teicoplanin-like GP1416 from *Amycolatopsis* sp. WAC 01416)[40]. Although the vast majority of these GPA producers belong to the *Amycolatopsis*[55] genus, our recent research indicated that GPA producers could be found among lesser-known genera of *Pseudonocardiales*, such as *Actinokineospora*[52].

Thanks to the comparative analysis of the available *Pseudonocardiales* genomes, in this work we reported the identification of two GPA BGCs with unusual NRPS properties, respectively in the genomes of *Actinokineospora auranticolor* YU 961-1 (=DSM 44650) and of *Umezawaea endophytica* DSM 103496. Intriguingly, in both cases the specificity of the NRPS module 3 (M3) adenylation (A)-domains could not be unambiguously predicted by bioinformatics tools. Further experimental investigation of *A. auranticolor* DSM 44650 confirmed that this strain actively produces an unknown GPA complex. Surprisingly, we discovered that GPA productivity in *A. auranticolor* DSM 44650 was in the unexpected range of 0.7–1.3 g L^{-1} in the commonly used R5 medium. Consequently, we isolated this bioactive GPA complex and characterized it using liquid chromatography-mass spectrometry (LC-MS) and high-resolution tandem mass spectrometry (MS/MS). The structure of the main congener was resolved using nuclear magnetic resonance (NMR) spectroscopy, revealing a novel aglycone type consisting of an aromatic AA1 and an aliphatic AA3. GPA complex produced in *A. auranticolor* DSM 44650 was named kineomicins. Elucidated structure of kineomicins appears to be the first example of a different type of GPAs, transitional between Type I and Type II. Further investigations allowed us to characterize the corresponding biosynthetic gene cluster, *knm*, and to propose an integrated model for kineomicins biosynthesis.

Results and discussion

Harnessing the potential of *Pseudonocardiales* spp. to produce GPAs with novel peptide scaffolds

At the time of our research (2023), GenBank contained up to 600 genomic records for *Pseudonocardiales* spp., which were available either as complete assemblies or as drafts of different quality (https://www.ncbi.nlm.nih.gov/assembly/?term=pseudonocardiales). We screened these genomic records using MultiGeneBlast[56] with the sequences of *bbr, oxyA, oxyB*, and *oxyC* from the balhimycin BGC (*bal*) as query-probes. Nucleic acid sequences containing co-localized BLAST hits were further subjected to antiSMASH 7.0[57] to identify BGCs. As a result, we identified 40 genomic records potentially encoding for GPA BGCs (Supplementary Table 1) which might be attributed to 35 different strains belonging to *Pseudonocardiales* order. Some of these BGCs were already known and described previously[41,52]. Notably, in addition to several species of *Amycolatopsis* (carrying BGCs for Types I-IV GPAs, Supplementary Table 1) and two species of *Kibdelosporangium* (carrying BGCs for Type I chloroeremomycin and for an unknown Type II GPA), we found that poorly known genera as *Actinokineospora*, *Kutzneria*, and *Umezawaea* might produce GPAs as well, further expanding the range of putatively GPA-producing *Pseudonocardiales* spp. Phylogenetic relationships of these strains are illustrated by Supplementary Fig. 2.

We then placed the 35 identified BGCs into a phylogenetic framework by building a multi-locus phylogeny (MLP) (Fig. 1). Concatenated sequences of a conserved set of proteins encoded in each GPA BGC from *Pseudonocardiales* spp. described to date were used, including: an ABC-transporter (orthologue of Tba coded in *bal*[58]); the crosslinking oxygenases that install *A-B*, *C-O-D*, and *D-O-E* crosslinks in type I-IV GPAs (orthologues of OxyA, OxyB, and OxyC coded in *bal*[19]); and the β-hydroxytyrosine (Bht), 4-hydroxyphenylglycine (Hpg), and 3,5-dihydroxyphenylglycine (Dpg) biosynthetic enzymes (orthologues of Bhp, BpsD, HmaS, DpgA, DpgB, and DpgC coded in *bal*[32,33,59,60]) (Supplementary FASTA File 1). This concatenation was possible for 33 out of the 35 investigated BGCs, since the sequences for two of them (Supplementary Table 1) were incomplete and missing the corresponding genes.

In the further analyses, the organization of NRPSs encoded within each BGC, their A-domain specificities, and the presence of different cross-linking oxygenases, were compared by extrapolating this information from the genomic data and correlating it with phylogeny (Fig. 1, Supplementary Table 2). Then, the repertoire of the tailoring genes (i.e., halogenases, methyltransferases, glycosyltransferases, sulfotransferases, and acyltransferases) found in each BGC (Supplementary Table 2) was analyzed. The amino acid composition of each peptide scaffold, together with their cross-linking patterns, were predicted, and each BGC was assigned to the currently known GPA Types. The result was that well-separated clades of the tree coherently grouped the BGCs coding for the biosynthesis of structurally similar GPAs (Fig. 1).

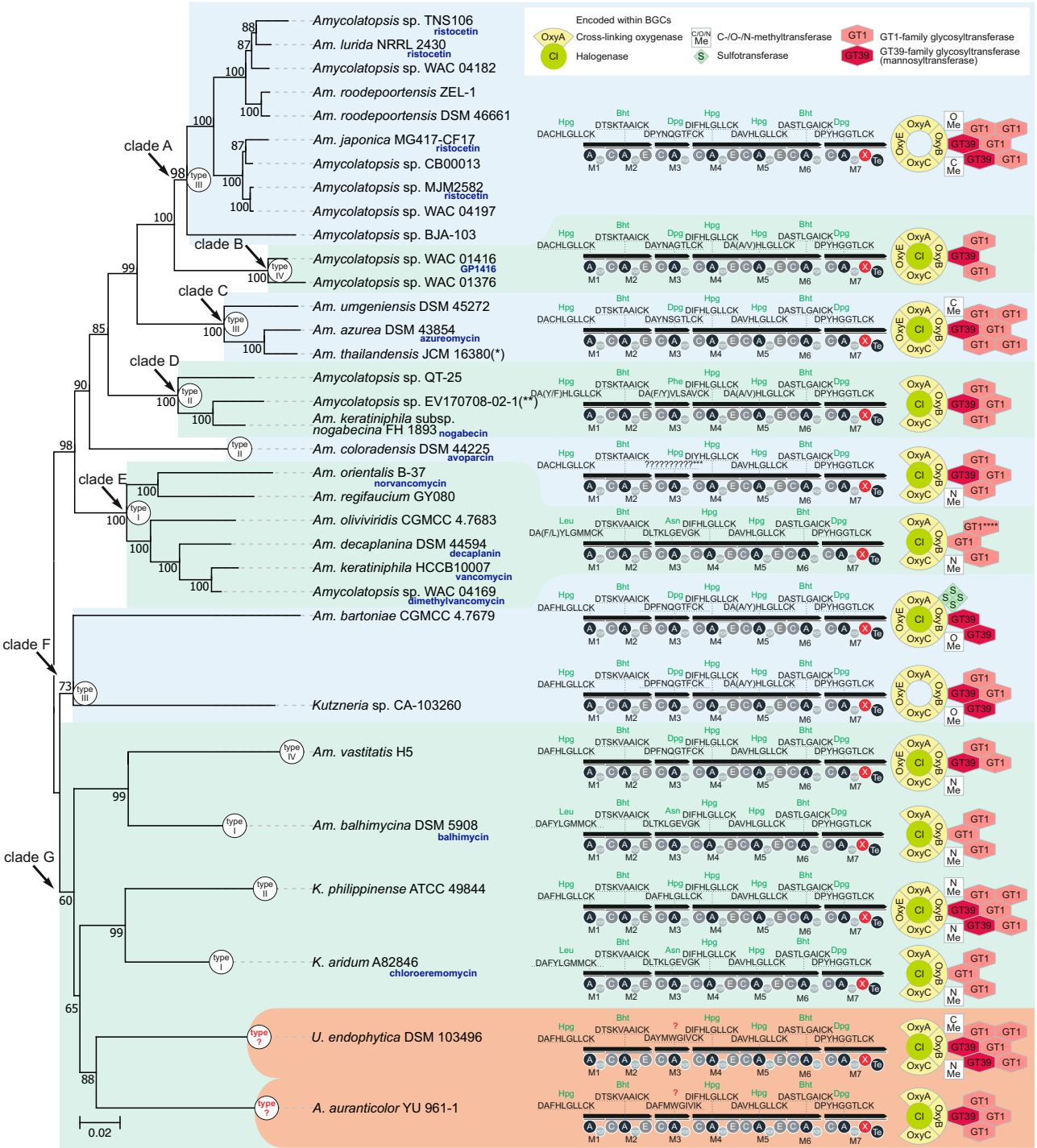

* only three GT1 genes found (likely due to BGC sequence fragmentation); *C*-methyltransferase gene not found (likely due to BGC sequence fragmentation).
** one GT1 gene found frameshifted.
*** was impossible to infer non-ribosomal code due to poor sequence quality.
**** third GT1 gene found only in GY080, CGMCC 4.7683, DSM 44594.

Fig. 1 | Unifying scheme describing the diversity of the GPA BGCs found in *Pseudonocardiales* spp. On the left side, the MLP of the 33 GPA BGCs selected from the genomic records of *Pseudonocardiales* spp. (see Supplementary Table 1) is represented: concatenated protein sequences of central biosynthetic enzymes encoded in each BGC (see main text) were used to build the unrooted maximum-likelihood phylogenetic tree (bootstrap values of branch support analysis were obtained from 500 replicates). The names of the GPAs are reported under the species previously known to produce them. To the right, the predicted domain architecture of each NRPS (where the non-ribosomal codes are given) is reported, as well as the schematic representation of monooxygenases and of the other tailoring enzymes taking part in post NRPS biosynthetic steps, coded within the corresponding BGCs (see Supplementary Table 2).

Clade A (Fig. 1) included the BGCs from the already known Type III GPA ristocetin producers (*Amycolatopsis lurida* NRRL 2430, *Amycolatopsis japonica* MG417-CF17, *Amycolatopsis* sp. MJM2582, and *Amycolatopsis* sp. TNS106[21,39,54], further denoted as *ris* BGCs) and all the BGCs predicted by us or other authors[41] that appeared identical to those of the known producers (Supplementary Fig. 3). Coherently, these BGCs lacked genes for halogenases, since the corresponding GPAs are not halogenated (Supplementary Table 2). The sister clade B (Fig. 1) grouped two BGCs identical in terms of

genetic organization (Supplementary Fig. 3) that code for the biosynthesis of teicoplanin-like acylated GPAs: the product from one of them (known as GP1416) was previously identified from *Amycolatopsis* sp. WAC 01416[40]. Clade C (Fig. 1) contained three BGCs respectively from the azureomycin producer *Amycolatopsis azurea* DSM 43854[61] and from two other *Amycolatopsis* spp. still not known to produce GPAs. Of note, the structure of azureomycin is still unresolved. These BGCs seemed identical in terms of genetic organization (Supplementary Fig. 3). Their predicted products would be Type III GPAs, although the repertoire of glycosyltransferases (GTFs) coded by their BGCs is more limited than in *ris* BGCs, and halogenase genes are present (Supplementary Table 2). Clade D (Fig. 1) included the known producer (*Am. keratiniphila* ssp. *nogabecina* FH 1893) of the Type II GPA nogabecin and two additional identical BGCs from two other *Amycolatopsis* spp. (Supplementary Fig. 3). Interestingly, the BGC sequence for the Type II GPA avoparcin from *Am. coloradensis* DSM 44225 appeared as an outgroup to clades A, B, and C. Unlike nogabecin-like Type II GPAs, avoparcin carries Hpg instead of Phe in AA3 position[1], indicating its different origin and its unrelatedness to clade D Type II GPA BGCs (confirmed by the different genetic organization, Supplementary Fig. 3). Clade E grouped the vancomycin-like BGCs coding for Type I GPAs including vancomycin and norvancomycin (Fig. 1 and Supplementary Fig. 3), the BGCs for decaplanin from *Amycolatopsis decaplanina* DSM 44594[62], and for dimethylvancomycin from *Amycolatopsis* sp. WAC 04169[8].

The last two clades of the tree, F and G, were much more sparsely populated and included many putatively novel BGCs. In clade F, two BGCs were present (Fig. 1), likely coding for Type III GPAs, but different from those grouped in clades A and C due to their repertoire of tailoring genes (Supplementary Table 2, Supplementary Fig. 3). Notably, one of these BGCs was found in the genome of *Kutzneria* sp. CA-103260[63], although members of this genus were not previously known to produce GPAs. The second was unusual GPA BGC of *Amycolatopsis bartoniae* CGMCC 4.7679 (Supplementary Fig. 3)[64]. Clade G grouped BGCs for GPAs of different types (Fig. 1 and Supplementary Fig. 3), including well known BGCs as the ones encoding for Type I balhimycin (*bal*) and chloroeremomycin BGC (*cem*). Sequences from *bal* formed a subclade with sequences from the *Amycolatopsis vastitatis* H5 BGC, which, on the basis of our analyses, likely codes for the biosynthesis of a yet unknown Type IV GPA. At the same time, sequences from *cem* grouped together with sequences from *Kibdelosporangium philippinense* ATCC 49844 BGC, which putatively codes for the biosynthesis of a novel Type II GPA, carrying a Hpg residue in the AA3 position.

Finally, the last G subclade included the BGCs from *Actinokineospora auranticolor* YU 961-1 (=DSM 44650) and *Umezawaea endophytica* DSM 103496, and for both of them we found impossible to predict the specificity of the A-domain from NRPS M3. The non-ribosomal code of the M3 A-domain from *U. endophytica* DSM 103496—DAYMWGIVCK—was never reported before and it shared the highest similarity with the code (DAYLWGGVFK) found in the A-domain of KtzE (ABV56585) from kutzneride biosynthesis[65], which is specific for incorporating a unit of 2-(1-methylcyclopropyl)-D-glycine[65]. In the case of *A. auranticolor* YU 961-1, the code of the M3 A-domain (DAFMWGIVIK) was also previously unknown and shared the highest similarity to the code (DAFWWGGVFK) found in the M3 A-domain of ecumicin biosynthesis NRPS (AIW58892)[66] from *Nonomuraea* sp. MJM5123, where it was found specific for L-*allo*-isoleucine[66]. Thus, the GPA NRPSs from *U. endophytica* DSM 103496 and *A. auranticolor* YU 961-1 represent the unique cases so far described, where the A-domain of M1 recognizes the aromatic amino acid (Hpg), while the M3 A-domain likely recognizes an aliphatic amino acid. To the best of our knowledge, such recognition pattern is unprecedented among the biosynthetic pathways of known GPAs, and the corresponding compounds do not actually fit into the existing classification of GPAs types[1], thus requiring its update.

Driven by the novelty of the predicted chemical structures, our efforts were then devoted to the investigation of putative GPA production in *A. auranticolor* YU 961-1 and *U. endophytica* DSM 103496 with the goal to purify and characterize these yet-unknown compounds. In this paper, we focused on *A. auranticolor* YU 961-1 (=DSM 44650), as our preliminary studies demonstrated that this strain produced the putative GPA at high level in standard cultivation conditions (see below). GPA production in *U. endophytica* DSM 103496 will be instead investigated in future.

GPA production in *A. auranticolor* DSM 44650

To the best of our knowledge, *A. auranticolor* DSM 44650 was never tested before for GPA production[67]. Therefore, we grew the strain at Erlenmeyer flask scale in a range of vegetative and production media using *Bacillus subtilis* HB0950[68] as an indicator strain. The latter strain might serve as an antimicrobial assay system in which lipid II binders, including GPAs, induce the chromogenic conversion of X-Gal (5-bromo-4-chloro-3-indolyl-β-D-galactopyranoside) at the edge of the growth inhibition zone[69,70]. Through this assay, we discarded several media (VSP[71], TM1[72], FM2[71], YMPG[73], ISP2[74], GYM *Streptomyces* medium[75], GYC[76], and SG[77]) since no GPA-related antimicrobial activity (or only a weak one) was detectable. On a contrary, *A. auranticolor* DSM 44650 gave a clearly green-blue edged antimicrobial inhibition halo when cultivated in TSB[78], Lysogeny broth (Miller), SAM[79], and liquid R5 medium[78] (Supplementary Fig. 4). This last one, which was previously used for the routine production of balhimycin[35,80,81] and ristocetin[21], seemed to allow the highest production of the putative antibiotic, and was, therefore, selected for the subsequent cultivations of *A. auranticolor* DSM 44650 at flask and bioreactor scale (Fig. 2a, Supplementary Fig. 5, Supplementary Data 1).

A. auranticolor DSM 44650 grew in R5-containing flasks, reaching the maximum biomass production (48.6 ± 3.2 g L^{-1} in dry weight) after 192 h of cultivation (Fig. 2a, Supplementary Data 1). Glucose was slowly consumed during the microbial growth, being completely depleted after 264 h from the inoculum, whereas pH tended to remain stable in the 7.0-7.5 interval for the entire cultivation time (Fig. 2a, Supplementary Data 1). Putative GPA production was detected by the photodiode-array (PDA) HPLC of day-by-day culture extracts (Fig. 2b, Supplementary Data 1). Starting from 24 h of cultivation, several peaks at various retention times (t_R) and showing UV spectra with high similarity to those from GPA standards (e.g., vancomycin and teicoplanin), became detectable (Fig. 2c), indicating that *A. auranticolor* DSM 44650 produces, as in the case of many other GPAs[1], a complex of structurally related congeners. We named this putative GPA complex kineomicins (from the name of the producing strain *Actinokineospora*, Kmc). Four major peaks were identified (named KmcA-KmcD), with KmcB being the most abundant congener, together with other structurally related minor components (Fig. 2b, c). Kmc production started during the exponential growth phase but reached its maximum during the stationary phase, then remaining almost stable till the end of cultivation—336 h after the inoculum (Fig. 2b, Supplementary Data 1). A slightly different growth curve and production time course were observed at the level of 3-L bench bioreactor cultivation, where biomass accumulation followed a diauxic profile (Supplementary Fig. 5a) and Kmc production continued to increase up to the end of the cultivation at 336 h (Supplementary Fig. 5b). Notwithstanding these differences, the same kineomicin complex composition, with four major peaks (KmcA-KmcD) and various other minor congeners, was highlighted by PDA-HPLC analyses also at bioreactor level (Supplementary Fig. 5b, c). The total Kmc productivity (calculated as the sum of the major and minor congeners detectable by PDA-HPLC) indicated a maximum productivity of 685 ± 95 mg L^{-1} after 288 h of cultivation at flask level (Fig. 2b, Supplementary Data 1) and of 1320 ± 280 mg L^{-1} at bioreactor scale after 336 h (Supplementary Fig. 5b).

Initial attempt to purify Kmc from culture extracts using the D-Ala-D-Ala affinity chromatography indicated that the four main congeners bound to the functionalized resin, which mimics the canonical GPA target in the bacterial cell wall[82], confirming their dalbaheptide mode of action (Fig. 2d). This preparation was also tested for its antimicrobial activity, measuring minimum inhibitory concentrations (MICs) and minimal bactericidal concentrations (MBCs)[83] against a collection of clinically relevant Gram-positive and Gram-negative bacteria, in parallel with vancomycin and

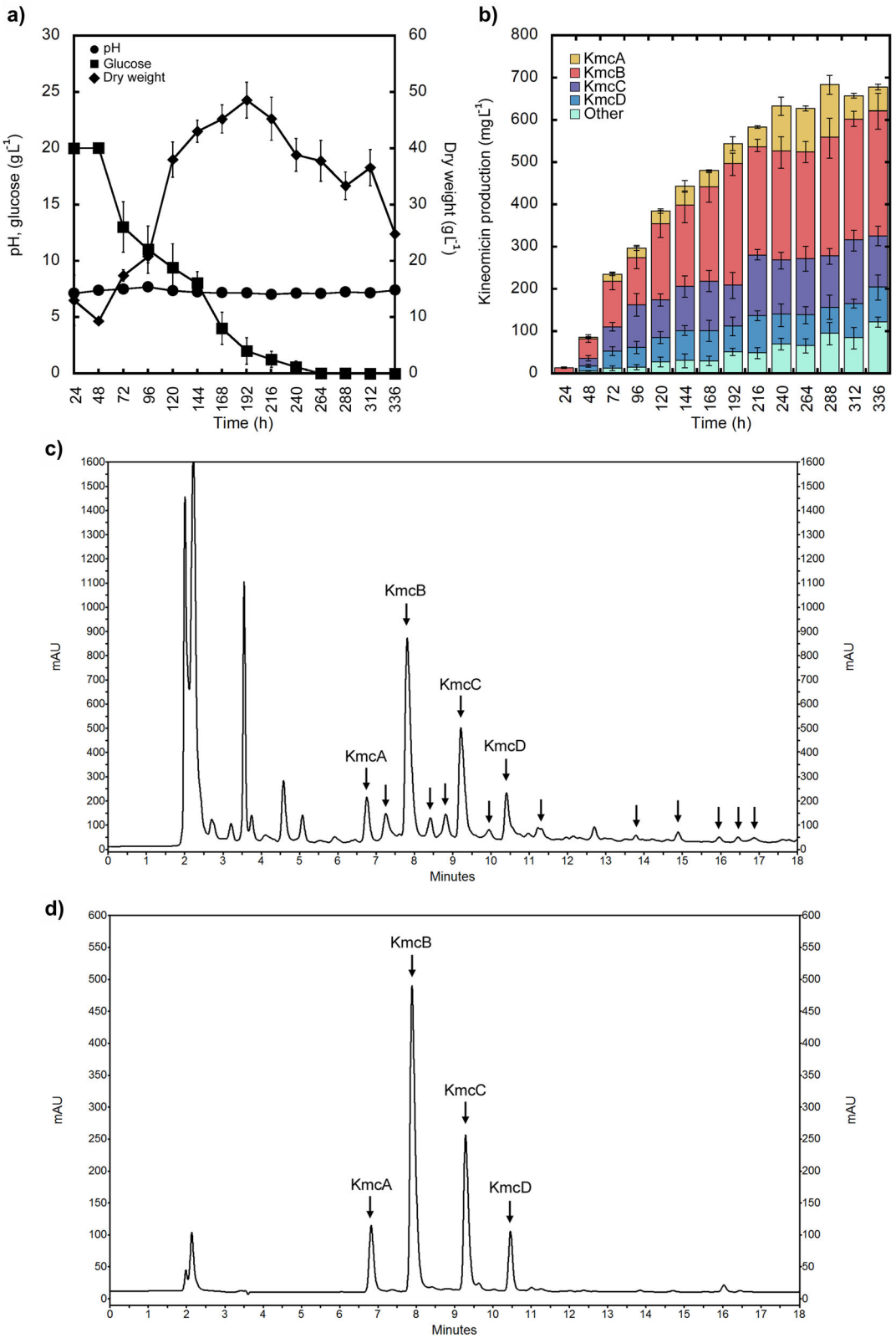

Fig. 2 | *A. auranticolor* DSM 44650 growth and kineomicin complex production at flask level. a, **b** Time course of *A. auranticolor* DSM 44650 growth (**a**) and production of Kmc congeners (**b**) in R5 medium at 500 mL Erlenmeyer flasks-scale. pH (circles, **a**), residual glucose (squares, **a**), dry weight (rhombi, **a**) Kmc total production and complex composition by PDA-HPLC analyses (**b**) were monitored every 24 h. Results provided are mean values of seven independent experiments ± standard deviations. In panel (**b**) all minor components of Kmc complex are grouped as "other". **c**, **d** HPLC chromatograms (λ = 236 nm detection wavelength, see the methods section for details) of a culture extract from *A. auranticolor* DSM 44650 cultivated for 336 h in R5 medium (**c**) and of a partially purified fraction from the same extract following D-Ala-D-Ala affinity chromatography (**d**). In both panels, arrows indicate major (KmcA, KmcB, KmcC, and KmcD) and minor peaks attributable to the different congeners of Kmc complex.

Table 1 | Minimum inhibitory concentrations (MICs) and minimal bactericidal concentrations (MBCs) of Kmc in comparison to the clinically-approved first-generation GPAs vancomycin and teicoplanin

Strain	Kineomicin		Vancomycin		Teicoplanin	
	MIC (μg mL^{-1})	MBC (μg mL^{-1})	MIC (μg mL^{-1})	MBC (μg mL^{-1})	MIC (μg mL^{-1})	MBC (μg mL^{-1})
Staphylococcus aureus ATCC 6538 P (MSSA)	2	4	1	4	0.5	4
Staphylococcus aureus ATCC 25923 (MSSA)	0.5	2	0.5	2	0.5	2
Staphylococcus aureus ATCC 43300 (MRSA)	2	8	2	8	1	16
Staphylococcus haemolyticus 3902	8	>128	2	16	32	64
Staphylococcus epidermidis strain 4	2	64	4	16	4	64
Enterococcus faecalis ATCC 29212	4	8	2	32	1	64
Enterococcus faecalis ATCC 51299 (VanB)	16	>128	8	>128	2	32
Enterococcus faecalis 9160188401-EF-34 (VanA)	>128	>128	128	>128	32	>128
Escherichia coli ATCC 35218	>128	>128	>128	>128	>128	>128
Moraxella catarrhalis ATCC 3293	>128	>128	>128	>128	>128	>128

Values represent the average of the data from at least three independent experiments. According to the Clinical and Laboratory Standards Institute, strains can be classified as susceptible (MIC ≤ 2 μg mL^{-1}), intermediate resistant (4 ≤ MIC ≤ 8 μg mL^{-1}), or resistant (MIC ≥ 16 μg mL^{-1})[83].

teicoplanin (Table 1). Kmc showed the typical GPA antimicrobial spectrum, targeting Gram-positive bacteria (staphylococci and enterococci), but not the Gram-negative *Escherichia coli* ATCC 35218 and *Moraxella catarrhalis* ATCC 3293. Kmc, albeit tested as a still not completely purified extract, was particularly effective versus staphylococci, including methicillin-resistant *Staphylococcus aureus* ATCC 43300 (MRSA), and the clinical isolates *Staphylococcus epidermidis* strain 4 and *Staphylococcus haemolyticus* 3902, when compared to the pure standards of vancomycin and teicoplanin. On enterococci, the antimicrobial activity of Kmc was overall lower than on staphylococci, being, as vancomycin, ineffective on the clinical isolate with VanA phenotype *Enterococcus faecalis* 9160188401-EF-34 and on VanB-type *E. faecalis* ATCC 51299, but showing MBCs lower than those of vancomycin and teicoplanin towards *E. faecalis* ATCC 29212 (Table 1).

These results confirm that *A. auranticolor* DSM 44650 synthetizes a GPA complex with a promising antimicrobial activity and produces it at a remarkable level. For example, balhimycin productivity in the model *Am. balhimycina* DSM 5908 (cultivated in R5 and other media) ranged from *ca.*100 to 250 mg L^{-1} [84–86]. Ristocetin production in wild type strains reached around 100 mg L^{-1} [54]. In non-*Pseudonocardiales* GPA producers, antibiotic production levels in optimized production media may vary in the range of *ca.* 200–300 mg L^{-1} (e.g., teicoplanin production in *Act. teichomyceticus* ATCC 31121 or A40926 production in *N. gerenzanensis* ATCC 39727)[46,72]. Only GPA overproducers, generated through gene-engineering or classical mutagenesis and selection, have the potential to yield antibiotics in grams per liter range[87–89]. In this context, *A. auranticolor* DSM 44650 stands out as a unique naturally tailored GPA overproducer and for this reason it might also be considered in future as an alternative platform for the production of heterologous GPAs.

Characterization of kineomicin complex and structure elucidation of kineomicin B

Production of Kmc complex in *A. auranticolor* DSM 44650 culture extracts was then investigated by HPLC-ESI-HRMS detecting a set of structurally related ions (Supplementary Fig. 6, Supplementary Table 3). $[M + H]^+$ of KmcA-KmcD were *m/z* 1698.5786, 1712.5990, 1729.5773, and 1713.5826, respectively, and corresponded to the four major congeners. In addition, a group of thirteen minor components were identified by LC-MS (Supplementary Fig. 6, Supplementary Table 3). The most abundant KmcB congener (*m/z* of 1712.5990) displayed characteristics consistent with the presence of one chlorine atom, as discerned from the HR-MS isotope distribution pattern[20], a typical modification found in GPAs. KmcB was then purified from the producing cultures of *A. auranticolor* DSM 44650 cultivated in R5 medium for 288–336 h, by D-Ala-D-Ala affinity chromatography[90] followed by reverse phase HPLC (Supplementary Fig. 7), yielding 6.1 mg of a white solid. Data interpretation from 1D/2D NMR spectra revealed that KmcB is composed of seven amino acids (as other Type I-IV dalbaheptides) with discernible δ ($^1H_\alpha$) values at 4.32, 4.61, 4.05, 5.54, 4.46, 4.21, and 4.34 ppm (Supplementary Fig. 8, Supplementary Table 4)[20]. Further investigation by means of ^{1}H-^{13}C HSQC, ^{1}H-^{1}H COSY, ^{1}H-^{1}H TOCSY, and ^{1}H-^{13}C HMBC (Supplementary Figs. 9, 10, 11, and 12, respectively) identified these amino acids as 4-hydroxyphenylglycine (^{1}Hpg), β-hydroxytyrosine (^{2}Bht), isoleucine (^{3}Ile), two cross-linked Hpg residues (^{4}Hpg-^{5}Hpg), β-OH-3-Cl-tyrosine (^{6}Bht), and one crosslinked 3,5-dihydroxyphenylglycine (^{7}Dpg). Notably, the cross-links occur between ^{5}Hpg and ^{7}Dpg, via a carbon-carbon bond, and between ^{2}Bht and ^{4}Hpg, and ^{4}Hpg and ^{6}Bht, mediated by aryl ether bonds, as confirmed by HSQC, HMBC, and NOESY spectra (Supplementary Figs. 9, 12, and 13, respectively). Moreover, four glycosyl residues were identified by 2D-NMR analysis: α-mannose, α-ristosamine, and a β-glucosyl-α-ristosaminyl disaccharide attached to residues ^{7}Dpg, ^{6}Bht, and ^{4}Hpg, respectively (Supplementary Fig. 14a), thus completing the 2D structure elucidation of the novel GPA KmcB (Fig. 3a, b, and Supplementary Fig. 15). The molecular formula of $C_{80}H_{94}ClN_9O_{31}$ deduced from the NMR experiments is in agreement with the molecular formula determined by HPLC-ESI-HRMS measurements for KmcB (Supplementary Fig. 16a), and the resulting structure of KmcB is also in full agreement with MS/MS data (Supplementary Fig. 16b)[90].

Confirming what highlighted by genomic analyses and phylogenetics, KmcB is therefore a peculiar GPA with a novel heptapeptide aglycone type containing an aromatic amino acid (Hpg) in AA1 and an aliphatic (isoleucine) in AA3. Such configuration is transitional between Type I vancomycin-type dalbaheptides (both AA1 and AA3 aliphatic) and Type II dalbaheptides such as avoparcin and keratinimicin (AA1 and AA3 aromatic).

Despite this, it remained to establish the absolute configuration of ^{3}Ile in KmcB, that was conclusively established utilizing the advanced Marfey's method. Following hydrolysis (6 N HCl, 110 °C, 12 h) of KmcB, the resultant mixture underwent D/L-FDLA derivatization and subsequent analysis via HPLC-ESI-HRMS mass spectrometry. The obtained data unequivocally indicated the presence of ^{3}Ile residue in the L-configuration (Supplementary Fig. 17)[91]. Therefore, we can conclude that the novel non-ribosomal code of Kmc M3 A-domain—DAFMWGIVIK—is specific for L-Ile. Finally, utilizing bioinformatics-based A-domain specificity prediction, the assignment of chiral centers for the other amino acids was performed[57], thus finalizing the proposed structure of KmcB, as illustrated in Fig. 3c.

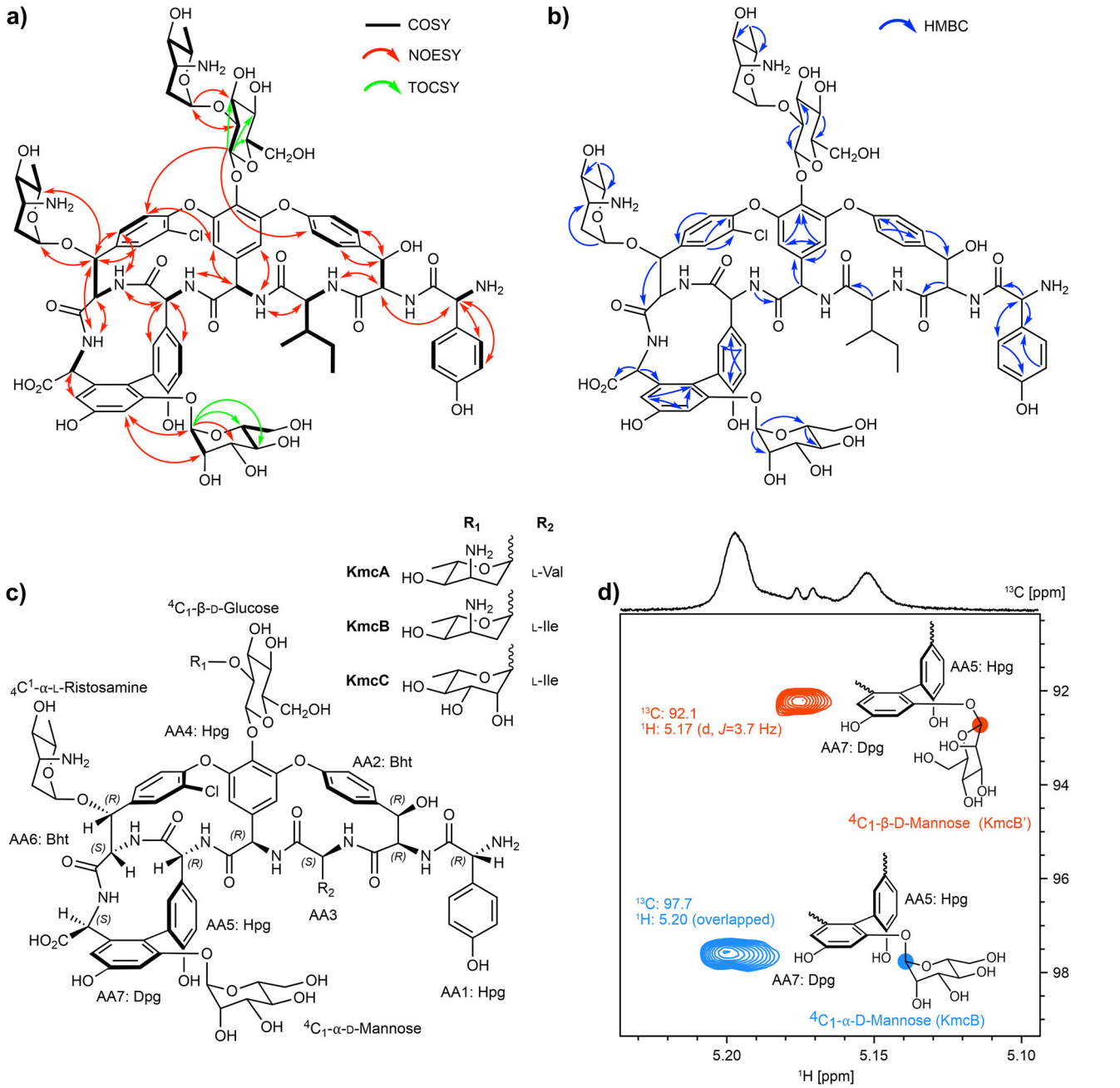

Fig. 3 | Structure elucidation of KmcB and KmcB'. a Key COSY/NOESY/TOCSY and (**b**) HMBC correlations are highlighted in the structure of KmcB. **c** Structures of KmcA-C with varying substitution patterns and assignment of the chiral centers. **d** ^{1}H-^{13}C HSQC section of KmcB with chemical shift ranges from 5.10–5.23 ppm (^{1}H) and 90.5–99.0 ppm (^{13}C) (DMSO-d_6, 298 K). The cross peaks belonging to the anomeric carbons within the mannose moieties in both KmcB (***blue***) and minor KmcB' (***red***) are annotated.

Interestingly, in the series of consecutive NMR measurements of KmcB, an additional set of signals was observed (Supplementary Fig. 18a). The analysis of these spectra facilitated the elucidation of a second compound (termed KmcB'). Notably, its chemical shifts closely resemble those of KmcB, with the exception of an alteration of 5.6 ppm in the chemical shift of the anomeric carbon of mannose (Supplementary Table 4), indicating a β-configurated mannose in KmcB' (Fig. 3d and Supplementary Fig. 14b)[92,93]. As in the ^{1}H-NMR spectra the peaks corresponding to KmcB did not show any significant decrease (Supplementary Fig. 18b), we explained this observation with a solubility effect or dimerization/monomerization during HPLC purification and analytics[94], rather than an isomerization during sample handling steps (e.g., rotary evaporation or lyophilization). This conclusion was also supported by the retention time detected of a new peak with the same MS patterns of KmcB (Supplementary Fig. 7b).

Although the structure of the three other main congeners of Kmc complex (KmcA, C, and D) was not accessed with NMR-spectrometry, further analysis of LC-MS and MS/MS data allowed us to speculate about the structures of KmcA and KmcC. Unfortunately, the quality of the MS/MS spectra for KmcD was not sufficient for its structure determination, due to low abundance. Thus, we assumed that KmcA differs from KmcB by carrying L-Val residue at AA3 (Supplementary Table 3, Supplementary Figs. 16 and 19), considering that the mass of KmcA is 14 Da smaller than that of KmcB, and such loss of a methyl group could not be apparently attributed to any other reaction during the biosynthesis of Kmc (see below).

Moreover, it is highly likely that the other major congener KmcC differs from KmcB (Supplementary Table 3, Supplementary Figs. 16 and 20) by carrying a D-rhamnose residue attached to AA4 D-glucose instead of L-ristosamine.

Kineomicin BGC and biosynthesis model

In parallel to the structure elucidation of KmcB, we analyzed the organization of the Kmc BGC (named *knm*), assigning the functions to *knm* genes in Kmc biosynthesis. As in the other known GPA BGCs[2], *knm* genes encode for the biosynthesis of the antibiotic scaffold including the supply of non-proteinogenic amino acids and the tailoring reactions, for the self-resistance protecting the producer during antibiotic production, for the cluster-situated regulatory genes, and for the export of the antibiotic. *knm* consists of 41 ORFs, the majority of them having orthologues in other *Pseudonocardiales* GPA BGCs, as exemplified by a comparison with the model *bal* and *ris* BGCs[54,95] (Table 2, Fig. 4a). Searching for clues to explain the natural high production levels of Kmc, we also completely sequenced and assembled the full genome of *A. auranticolor* DSM 44650 (yielding a single circular 8,488 kbp chromosome). In addition, by semi-quantitative reverse transcription-PCR (RT-PCR), we investigated the operon structure of *knm* and compared it with those of *bal* and *ris* (from *Amycolatopsis* sp. TNS106), which were the only ones so far described at the transcriptomic level from *Pseudonocardiales* spp.[54,95]. *knm* consists of 8 operons (*O1-8*) and 6 monogenic transcriptional units (Fig. 4b). Integrating all the data obtained from in silico analysis, transcriptional studies, and analytical chemistry, we thus build a streamlined model for Kmc biosynthesis, moving from genes to product, that is presented below.

Resistance. *knm* contains a complete set of GPA resistance (*van*) genes[52]. This includes orthologues of *vanHAX* genes—*knm1-3*, a *vanRS* two-component regulatory system – *knm4-5*, and an orthologue of *vanY* —*knm6* (Table 2, Fig. 4a). GPA resistance genes are organized as *O1* (*knm1-2-3* – *vanHAX*) and *O2* (*knm4-5* – *vanRS*), but *knm6* (*vanY*) exists as a single gene (Fig. 4b). Thus, *knm* combines the features of *bal* (carrying the *vanRS* operon and the *vanY* gene within the BGC) and of GPA BGCs from other *Pseudonocardiales* spp. (carrying only the *vanHAX* operon within the BGC, e.g., *ris*)[82] (Fig. 4a). If these genes are all expressed, they could probably confer a highly self-resistant phenotype to the producer strain which may contribute to its surprisingly elevated antibiotic productivity. The pattern of GPA resistance in *A. auranticolor* DSM 44650 would merit further investigation.

Pathway specific regulation and export. Like all other BGCs from *Pseudonocardiales* spp. (Supplementary Fig. 3), *knm* contains a single gene for the StrR-like pathway-specific regulator – *knm7R* (Table 2, Fig. 4a). Similar to the orthologue from *ris* BGC, *knm7R* is a monogenic transcription unit (Fig. 4a, b)[54]. The ABC transporter, coded by *knm9*, shares 77% of its amino acid sequence identity with the balhimycin exporter Tba, whose function was proved experimentally[58], and it is most likely responsible for the export of Kmc. *knm9* is co-transcribed with *knmA-B* NRPS genes (forming *O3*, Fig. 4b); in *bal* and *ris*, *knm9* orthologues were also shown to be co-transcribed with NRPS genes (Fig. 4a)[54,95].

Tyrosine supply. The Kmc aglycone is mainly composed of aromatic amino acids, including two residues of Bht, three Hpg residues, and one Dpg residue. Their biosynthesis requires tyrosine either as a direct or indirect precursor[84,86]. To meet the high demand for tyrosine, *knm* carries two genes of the shikimate pathway enzymes: *knm8* and *knm13*, coding for prephenate dehydrogenase (Pdh) and for 3-deoxy-D-arabinoheptulosonate 7-phosphate (Dahp) synthase, respectively (Table 2, Figs. 4b and 5). Notably, while Knm8 is an orthologue of Pdh from *bal*[84], Knm13 is an orthologue of Tei14* from teicoplanin BGC[22] (and not of $Dahp_{sec}$ from *bal*). Knm13 and Tei14* belong to a different evolutionary lineage than $Dahp_{sec}$ within the Superfamily I of Dahp synthases, PRK08763 and PRK09261[96], respectively. Peculiarly, such properties of *knm8* and *knm13* are also reflected in the positions of genes within the BGC. *knm8* is located just downstream the cluster-situated regulatory gene and forms a separate transcriptional unit (like its orthologues in *bal* and *ris*, Fig. 4a, b), while *knm13* is located between the monooxygenase genes (within the *O5* operon) contrary to the *bal* and *ris* BGCs, where Dahp synthase gene is found on the 3' boundary of the BGC (Fig. 4a). In addition to *knm13*, we found that the genome of *A. auranticolor* DSM 44650 carries two genes for PRK08763-like Dahp synthases (*V5P93_005139* and *V5P93_004074*, Fig. 5), while only one of them ($dahp_{prim}$) was previously reported in the genome of *Am. balhimycina* DSM 5908[86]. Moreover, the genome of *A. auranticolor* DSM 44650 carries two genes for Superfamily II of Dahp synthases (*V5P93_002217* and *V5P93_006080*, Fig. 5), while only one of them (*A3CE_RS0135135*) was found in the genome of *Am. balhimycina* DSM 5908 (*A3CE_RS0135135*)[86]. On the basis of these analyses, we might speculate that the extended repertoire of Dahp synthase genes found in the genome of *A. auranticolor* DSM 44650 contributes to its unusually high Kmc production rate.

Biosynthesis of Bht, Hpg and Dpg. The *knm* BGC contains the typical set of genes for the biosynthesis of non-proteinogenic amino acids found in *Pseudonocardiales* spp. GPA BGCs (Table 2, Fig. 4a). However, the gene for DpgD enoyl-CoA hydratase, which serves as an accessory enzyme to DpgB, is absent in *knm*, resembling the situation observed in pekiskomycin BGCs[8]. The Bht and Hpg biosynthetic genes (*knm22-23-24-25-26*) constitute the *O7*, although *knm21* (4-hydroxyphenylglycine transaminase, Hpgt) exists as monogenic transcriptional unit (Fig. 4a, b). In *ris* and *bal* BGCs, Bht and Hpg biosynthetic genes also belong to one operon, and both carry Hpgt genes as a separate transcriptional unit. In *knm*, Dpg biosynthesis genes (*knm33-34-35*) belong to the *O8*, where they are co-transcribed with some other biosynthetic genes (discussed below), resembling the organization of Dpg genes in *bal*[95], whereas in *ris*, the corresponding genes form a separate operon[54].

Biosynthesis of the aglycone. The features of the NRPS coded within *knm* were analyzed in previous sections. The module/domain organizations of KnmA-D corresponded to the experimentally resolved structure of KmcB (Figs. 1 and 3). Nevertheless, some of the Kmc congeners (KmcA, *vide supra*) likely carry L-Val residue at AA3 position of the aglycone (Supplementary Fig. 19). This evidence might suggest a certain promiscuity in the substrate specificity of the M3 A-domain in Kmc biosynthesis NRPS, or of the corresponding C-domain. Unusual structure of Kmc aglycone raised some additional questions about the evolutionary route of the NRPS. Previous works demonstrated that aliphatic amino acids in AA1 and AA3 positions of Type I GPAs appeared as a result of gradual evolution of M1 A-domain substrate specificity and due to larger recombination events exchanging M3, respectively[44]. However, it is unclear which of these two routes was followed by Kmc M3. To address this, we reconstructed the phylogeny of 363 A-domains and 312 C-domains coming from GPA NRPSs from 52 BGCs (Supplementary Table 5). As a result, sequence of the M3 A-domain of Kmc grouped with the counterpart from *U. endophytica* DSM 103496 and with the phenylalanine (Phe)-specific A-domains from Type II GPA NRPSs (from *Am. keratiniphila* ssp. *nogabecina* FH 1893, *Amycolatopsis* sp. EV170708-02-1, and *Amycolatopsis* sp. QT-25), altogether belonging to a larger clade with the sequences of Dpg-specific M3 A-domains (Supplementary Fig. 21). Unfortunately, the reconstruction lacked the M3 A-domain sequence of Type II GPA avoparcin BGC from *Am. coloradensis* DSM 44225 (Hpg-specific). A similar picture was obtained for the M3 C-domain phylogeny (Supplementary Fig. 22). Thus, according to the reconstructed phylogenies, Ile-specific M3 A-domain of Kmc NRPS, Phe-specific M3 A-domains of Type II GPAs, and Dpg-specific M3 A-domains of other GPAs share immediate common ancestor.

To reflect these findings and fit Kmc into the existing classification of GPAs, we propose herein to separate Type II into two subtypes: Type IIa and Type IIb. In this way, GPAs with aromatic AA1 and aliphatic AA3 (first

Table 2 | Characterization of the genes belonging to *knm* BGC and comparison with their orthologues from *bal* (balhimycin BGC from *Am. balhimycina* DSM 5908) and *ris* (ristocetin BGC from *Amycolatopsis* sp. TNS 106)

knm	*bal* (nucleic acid sequence identity)	*ris* (nucleic acid sequence identity)	Product (function)
knm1	*a*	*ORF1* (78%)	VanH (GPA resistance D-Lactate dehydrogenase)
knm2	*a*	*ORF2* (81,5%)	VanA (GPA resistance D-Ala-D-Lac ligase)
knm3	*a*	*ORF3* (82%)	VanX (GPA resistance D,D-dipeptidase)
knm4	$vnlS_{Ab}$ (86%)	*a*	VanS (GPA resistance two-component regulatory system sensor histidine kinase)
knm5	$vnlR_{Ab}$ (85%)	*a*	VanR (GPA two-component regulatory system sensor resistance response regulator)
knm6	$vanY_{Ab}$ (77%)	*a*	VanY (GPA resistance D,D-carboxypeptidase)
knm7R	*bbr* (85%)	*ORF4* (85%)	StrR-like transcriptional regulator (key pathway-specific regulator)
knm8	pdh_{sec} (80%)	*ORF5* (79%)	Pdh (prephenate dehydrogenase, tyrosine supply)
knm9	*tba* (85%)	*ORF6* (84%)	ABC-transporter (GPA export)
knmA	*bpsA*	*ORF7*	NRPS (modules 1-2)
knmB	*bpsB*	*ORF8*	NRPS (module 3)
knmC	*bpsB*	*ORF9*	NRPS (modules 4-5-6)
knmD	*bpsC*	*ORF10*	NRPS (module 7)
knm10	*mbtH* (91%)	*ORF11* (92%)	MbtH (NRPS chaperone protein)
knm11	*oxyA* (83%)	*ORF12* (79%)	OxyA (cross-linking oxygenase, *D-O-E*)
knm12	*oxyB* (85%)	*ORF14* (82%)	OxyB (cross-linking oxygenase, *C-O-D*)
knm13	*a*	*a*	Dahp (3-deoxy-D-arabinoheptulosonate 7-phosphate) synthase, Tei14* orthologue (76% nucleic acid sequence identity) (tyrosine supply)
knm14	*oxyC* (84%)	*ORF15* (79%)	OxyC (cross-linking oxygenase, *A-B*)
knm15	*bhaA* (89%)	*a*	Tyrosine halogenase
knm16	*bgtfA* (79%)	*ORF16* (71%)	GT1-family glycosyltransferase
knm17	*bgtfB* (80%)	*ORF17* (77%)	GT1-family glycosyltransferase
knm18	*bgtfC* (78%)	*ORF17* (75%)	GT1-family glycosyltransferase
knm19	*orf2* (75%)	*ORF21* (74%)	*N*-acetylglucosaminyl deacetylase
knm20	*a*	*ORF22* (82%)	GT39-family glycosyltransferase (mannosyltransferase)
knm21	*pgat* (87%)	*ORF24* (85%)	HpgT (4-hydroxyphenylglycine transaminase, Hpg/Dpg biosynthesis)
knm22	*bhp* (88%)	*ORF25* (83%)	Thioesterase (Bht biosynthesis)
knm23	*bpsD* (86%)	*ORF26* (84%)	Single-modular NRPS (Bht biosynthesis)
knm24	*oxyD* (87%)	*ORF27* (84%)	Monooxygenase (Bht biosynthesis)
knm25	*hmaS* (84%)	*ORF28* (84%)	HmaS (hydroxymandelate synthase, Hpg biosynthesis)
knm26	*hmo* (86%)	*ORF29* (83%)	Hmo (hydroxymandelate oxidase, Hpg biosynthesis)
knm27	*orf7* (85%)	*a*	Na^+-H^+ antiporter
knm28	*dvaA* (89%)	*ORF30* (88%)	dTDP-4-dehydro-6-deoxy-α-D-glucopyranose 2,3-dehydratase
knm29	*dvaE**	*ORF31* (88%)	C4-ketoreductase
knm30	*dvaB* (90%)	*ORF32* (88%)	dTDP-3-amino-2,3,6-trideoxy-4-keto-D-glucose transaminase
knm31	*dvaD* (87%)	*ORF33* (86%)	C5-epimerase
knm32	*a*	*a*	glucose-1-phosphate thymidylylransferase
knm33	*dpgA* (88%)	*ORF35* (87%)	DpgA (type III polyketide synthase)
knm34	*dpgB* (84%)	*ORF36* (79%)	DpgB (enoyl-CoA hydratase)
knm35	*dpgC* (87%)	*ORF37* (85%)	DpgC (3,5-dihydroxyphenylacetyl-CoA 1,2-dioxygenase)
knm36	*a*	*a*	Uncharacterized protein conserved in bacteria (DUF2336)
knm37	*a*	*a*	Porcine testicular carbonyl reductase (PTCR)-like

a – orthologue is absent.

* – nucleic acid sequence identity is not given since *dvaE* in *bal* is truncated.

example here being Kmc) would belong to Type IIa, while the GPAs with both AA1 and AA3 aromatic will form Type IIb.

The *knm* BGC encodes three cross-linking oxygenases: Knm11, Knm12, and Knm14. These oxygenases are orthologues to OxyA, OxyB, and OxyC of balhimycin biosynthesis, respectively. They install *D-O-E, C-O-D*, and *A-B* crosslinks in the Kmc aglycone. Additionally, a single *knm*-encoded halogenase (Knm15) adds chlorine to AA6 Bht of the aglycone. The substrate specificity of Knm15 is the same as that of Pek27 (pekiskomycin halogenase[8]), and both proteins are related (Supplementary Table 6 and Supplementary Fig. 23).

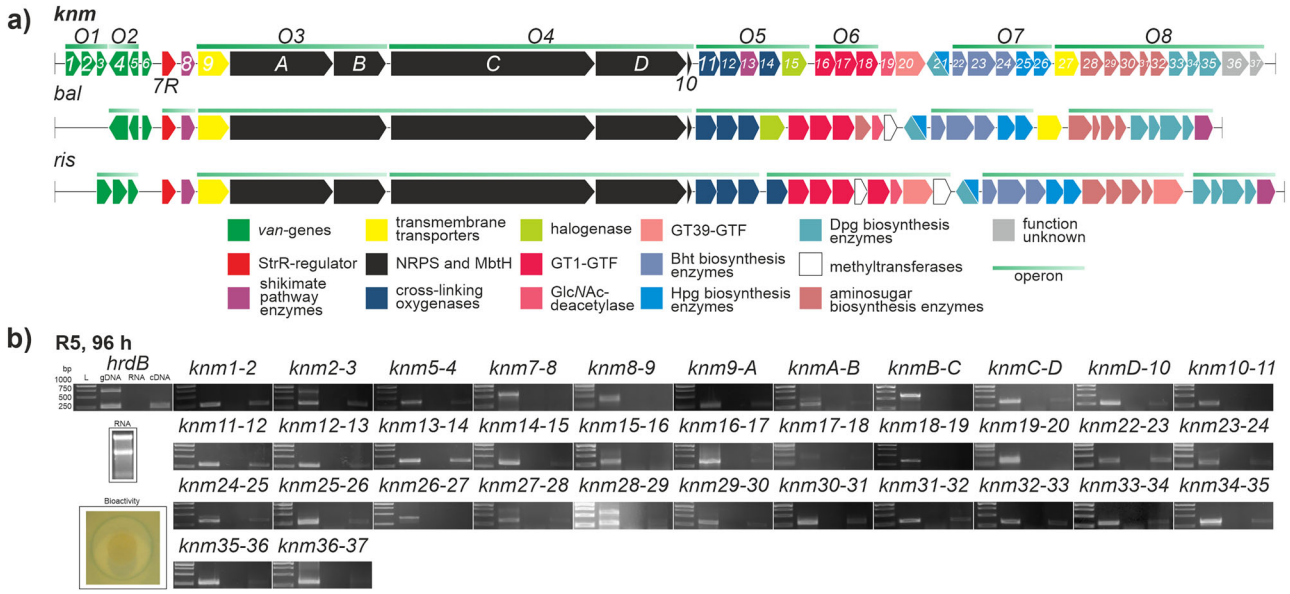

Fig. 4 | *knm* BGC in comparison with *bal* and *ris* BGCs and the operon structure of *knm*. **a** *knm* consists of 41 ORFs (resembling *bal* and *ris* BGCs, but lacking genes for methyltransferases). It is organized into 8 operons and 6 monogenic transcriptional units, according to (**b**) the results of semi-quantitative RT-PCR analysis showing the expression (or absence thereof) of all intergenic regions (35, except for the ones where neighboring genes lie on opposite strands and cannot be co-expressed) within *knm*. RNA was extracted from Kmc producing culture cultivated in R5 medium for 96 h, processed into cDNA, and used as a template for PCRs; chromosome DNA (gDNA) served as a positive control for each reaction, while non-treated RNA as a negative control; electrophoregrams represent the average results of three independent experiments.

The NRPS genes belong to the operons *O3* and *O4*; *knmA-B* are co-transcribed with *knm9* encoding for the ABC transporter (see above), and *knmC-D* are co-transcribed with *knm10* (MbtH, NRPS chaperone protein) (Fig. 4a, b). *O5* includes the genes *knm11-12-13-14-15*, coding for cross-linking oxygenases, Dahp synthase, and halogenase. Such organization shares some features with what observed in both *bal* (cross-linking oxygenase genes form a separate operon with halogenase gene, but all NRPS genes are co-transcribed) and *ris* (NRPS genes are divided into two separate operons, but the latter is extended with cross-linking oxygenase genes).

Ristosamine biosynthesis and glycosylation. *knm* contains a complete set of genes required for ristosamine biosynthesis (*knm28-32*, Table 2, Fig. 4a), three genes for GT1-family glycosyltransferases (GTFs) (*knm16-18*), and one gene for a GT39-family GTF (*knm20*) (Table 2, Fig. 4a). Since GT39-GTFs are mannosyltransferases[97], Knm20 is most likely responsible for the addition of the D-mannose residue to AA7 Dpg (similar to ORF22 in ristocetin biosynthesis[39]). Instead, to assign the functions to the three GT1-GTFs, we included them in a phylogenetic tree published earlier[98]. We found (Supplementary Table 7 and Supplementary Fig. 24) that Knm17 groups together with the GTFs installing D-glucose at AA4, while Knm16 groups with those that install an amino sugar at AA6. Thus, Knm17 most likely adds D-glucose at AA4 Hpg and Knm16 L-ristosamine at AA6 Bht (Fig. 5). This leaves Knm18 (grouping together with GTFs that add a second sugar residue to D-glucose at AA4, Supplementary Fig. 24) responsible for the addition of a second L-ristosamine residue to AA4 D-glucose in KmcB biosynthesis. As stated previously, at least some Kmc congeners (e.g., KmcC) likely carry a D-rhamnose instead of L-ristosamine attached to AA4 D-glucose (Supplementary Fig. 20). Since no other GT1-GTF genes were found in the genome of *A. auranticolor* DSM 44650, Knm18 most likely has an extended specificity to sugar donors, which has been also observed in keratinimicin biosynthesis[20].

The GT1-GTF genes (*knm16-17-18*) are co-transcribed as *O6*, while the mannosyltransferase gene (*knm20*) and the GlcNAc-deacetylase gene (*knm19*) form separate monogenic transcriptional units. Ristosamine biosynthesis enzymes (*knm28-29-30-31-32*) belong to the last operon (*O8*, the largest in the BGC), also including *knm27* (coding for Na^+/H^+-antiporter), *knm33-34-35* (Dpg biosynthesis enzymes, see above), as well as two genes with unclear function (*knm36-37*), apparently encoding proteins not relevant to GPA biosynthesis.

The biosynthetic model (Fig. 5) proposed from in silico analysis of *knm* and *A. auranticolor* DSM 44650 genome indicates that Kmc is produced following a scheme which is overall similar to the other GPAs produced by *Pseudonocardiales* spp. Anyhow, the notable differences which make Kmc unique are the following. First, the structural elucidation of the main congener KmcB demonstrated that it is a novel chemical structure (proposed as a model for the new chemical Type IIa of GPAs), with the heptapeptide aglycone containing Hpg in AA1 and L-Ile in AA3, this last incorporated due to the previously unknown code of the Kmc NRPS M3 A-domain, DAFMWGIVIK. Secondly, Kmc is produced as a complex of an unusually high numbers of congeners (at least 17 detected by LC-MS analyses, including the four major ones KmcA-D), demonstrating a high flexibility of the GPA biosynthetic machine of *A. auranticolor* DSM 44650. These congeners, in analogy with other GPA complexes[20,99], can be produced as intermediates during the biosynthesis, for example lacking some sugar residues/chlorine atoms added by post NRPS reactions, as reported in teicoplanin overproducing strains[100] and/or as degradation/detoxification products during GPA secretion (as in the case of recombinant strains producing increased amount of A40926[101,102]). A third peculiarity of Kmc, is, in fact, the elevated level of its production by the wild type strain: as a consequence, tailoring reactions might easily become bottleneck steps along the biosynthesis (thus leading to the observed heterogeneity of the complex), as well as detoxification reactions may be needed to sustain such high antibiotic productivity. *A. auranticolor* DSM 44650 genome analysis revealed that this naturally high producing phenotype is likely due to the expanded repertoire of Dahp synthase genes, which guarantee the aromatic amino acid supply for the aglycone synthesis, making this strain an interesting model for the heterologous production of GPA antibiotics. Finally, although further NMR studies are needed to confirm the structure of KmcA, if our prediction combining mass spectrometry data with in silico analysis of the BGC is correct, this specific congener might be produced due to the intriguing promiscuity of the M3 A-domain in the Kmc NRPS (supposed to introduce L-Val in KmcA instead if L-Ile in KmcB). To our knowledge, that

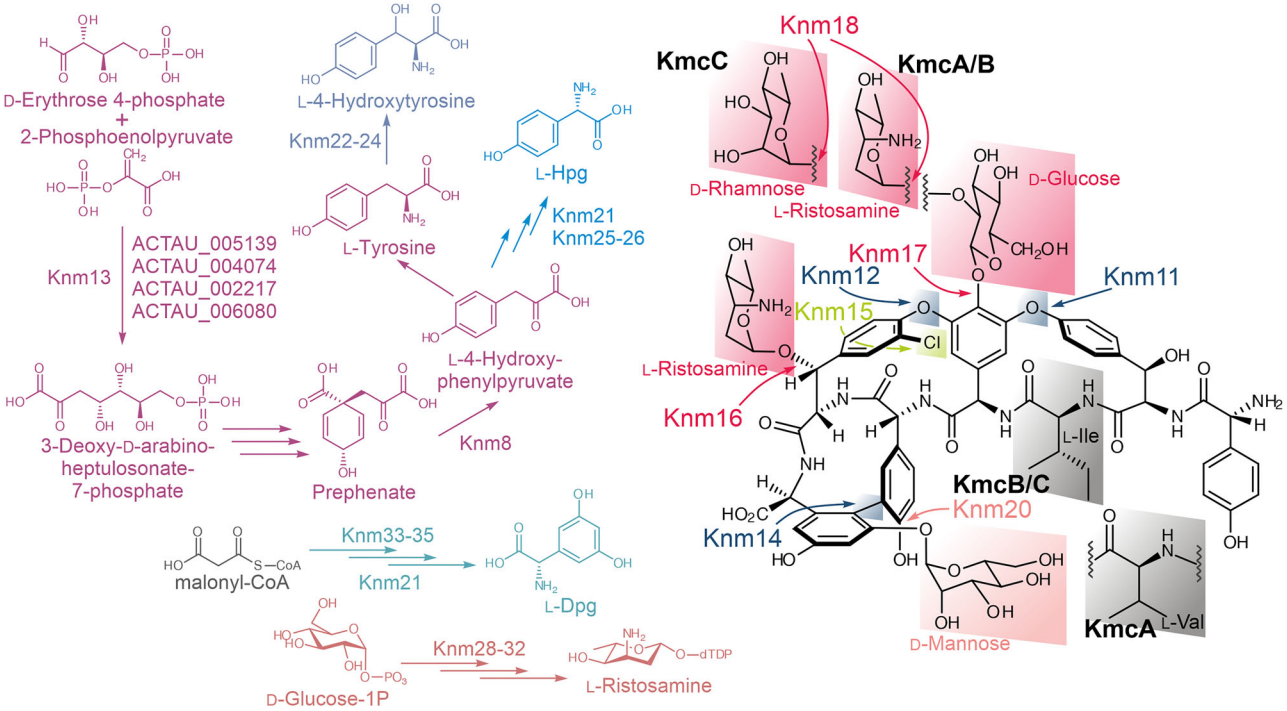

Fig. 5 | Reconstruction of Kmc biosynthesis. An integrated model for the Kmc biosynthesis assigning the roles to *knm* biosynthetic genes and to non-cluster encoded genes putatively involved in the precursor supply to produce KmcA-C.

would be the first case, in which a structural variation in a congener is generated during the assembling of the heptapeptide scaffold instead of being due to the peripheral tailoring reactions occurring on the already formed peptide[103]. The promiscuity of Kmc NRPS can open novel perspectives for reengineering the GPA aglycone assembling, generating a set of new variants. To this purpose, our future efforts will be devoted to the purification, structural elucidation and biological activity testing of the different congeners of Kmc, with the aim to identify the more active ones and eventually modulate their production by adapting cultivation conditions and/or engineering the BGC.

In conclusion, in this work we discovered a completely new GPA, that demonstrates yet another example of the pharmacophore-retaining evolutionary diversification of the ancestral teicoplanin-like aglycone[44]. These results open further insights into the chemical diversity of this clinically relevant antibiotic class and pave the way for developing in future new derivatives active on emerging resistant pathogens.

Methods

Bacterial strains and resources used in the work

Bacterial strains, used in the work, are listed in the Supplementary Table 8. Chemical substances, enzymes, cultivation media components, etc. are listed in the Supplementary Table 9.

Cultivation conditions of *A. auranticolor* DSM 44650

A. auranticolor DSM 44650 was routinely cultivated on solid YMPG medium[73]. Glycerol stocks of *A. auranticolor* DSM 44650, purchased from Leibniz Institute DSMZ (German Collection of Microorganisms and Cell Cultures), were prepared by growing the strain first in 50 mL of Tryptic Soy Broth (TSB) medium (g L^{-1} distilled water: 17 tryptone, 3 soya peptone, 5 NaCl, 2.5 K_2HPO_4, 2.5 dextrose, pH corrected to 7.3 before sterilization) in 300 mL Erlenmeyer flasks with *ca.* 10 glass beads (ø5 mm). After a 72 h incubation on a rotary shaker at 30 °C and 200 rotations per minute (rpm), 5 mL of the culture were transferred into 100 mL of the liquid version of YMPG medium (g L^{-1} distilled water: 2 yeast extract, 10 malt extract, 2 bacto peptone, 10 g glucose, 2 g KH_2PO_4, and 1 g $MgSO_4 \times 7H_2O$, pH corrected to 7.3 before sterilization)[73] in 500 mL flasks with *ca.* 10 glass beads (ø5 mm), then incubated for 96 h as above. Glycerol stocks were then prepared dividing the culture in 2-mL aliquots, stored at −80 °C with 10% *v/v* glycerol.

Cultivation of *A. auranticolor* DSM 44650 for Kmc production was initiated by inoculating one glycerol stock in 50 mL of SGC2 medium (g L^{-1} distilled water: 5 $CaCO_3$, 3 cane molasses, 5 casein hydrolysate, 30 soluble starch, 15 soya peptone, 15 dextrose, pH corrected to 7.0 before sterilization) in 300 mL Erlenmeyer flasks with *ca.* 10 glass beads (ø5 mm). After 72 h of incubation at 30 °C and 200 rpm, a 5% *v/v* inoculum was performed, transferring 5 mL of the culture into 100 mL of R5 medium[78] (g L^{-1} distilled water: 103 sucrose, 0.25 K_2SO_4, 10.12 $MgCl_2 \times 6\ H_2O$, 10 glucose, 0.1 casein hydrolysate, 5.73 TES buffer, 5 yeast extract, 2 mL trace element solution, 10 mL KH_2PO_4 solution at 0.5% *w/v*, 4 mL $CaCl_2 \times 2\ H_2O$ solution at 5 M, 15 mL L-proline solution at 20% *w/v*, 7 mL NaOH 1 N) in 500 mL Erlenmeyer flasks with *ca.* 10 glass beads (ø5 mm). The cultivation continued at 30 °C and 200 rpm for 336 h. Samples were collected every 24 h to estimate biomass accumulation (dry weight), pH (with a pH meter), glucose consumption (with Diastix sticks, Bayer AG, Leverkusen, Germany), and Kmc production (see below PDA-HPLC). For the cultivation in bioreactor, the culture of *A. auranticolor* DSM 44650 grown in SGC2 medium was used to inoculate at 5% *v/v* a 3-L P-100 Applikon glass reactor (height 250 mm, ø130 mm) equipped with an AD1030 Biocontroller and AD1032 motor, and containing 2 L of R5 medium, supplemented with 200 µL of Hodag antifoam (Hodag Chemical Corporation, Chicago, IL, US). Fermentation was carried out at 30 °C, with stirring at 400 rpm with Rushton blades and 2 L min^{-1} aeration rate. Dissolved oxygen (measured as % pO_2) was monitored using an Ingold polarographic oxygen electrode, while pH values were monitored using a pH meter. Foam production was controlled by adding Hodag antifoam through an antifoam sensor.

PDA-HPLC analyses

A. auranticolor DSM 44650 cultures were extracted by correcting their pH to 12.0 using NaOH 10 N, then centrifuged at 13,400 rpm for 15 min. Chromatographic analyses were performed with a VWR Hitachi diode array L-2455 HPLC system, with detection at 236 nm. 50 µL of each sample were injected onto a 5-µm-particle size KromaPhase 100 C18 4.6 × 250 mm HPLC column. Elution was done at a flow rate of 0.95 mL min^{-1}, with a

linear gradient from 5% *v/v* to 30% *v/v* of Phase B in 25 min. Phase A was 0.1% *v/v* phosphoric acid, while Phase B was 100% *v/v* HPLC-grade acetonitrile. Kmc production was quantified taking into consideration the areas of all major (KmcA-KmcD) and minor congeners identified by the UV spectrum, and using 50 µL of 50 µg mL^{-1} vancomycin as internal standard.

LC-MS and MS/MS analyses

LC-MS and MS/MS analyses were conducted using an LTQ-Orbitrap XL hybrid ion trap-orbitrap mass spectrometer (Thermo Fisher Scientific GmbH, Bremen, Germany) coupled with an analytical HPLC 1290 Infinity system (Agilent Technologies, Waldbronn, Germany). To analyze the culture extracts and crude extracts, an HPLC column (Poroshell 120, EC-C18, 50 × 2.1 mm, 2.7 µm, Agilent Technologies, Waldbronn, Germany) enabled the sample separation and was eluted by a linear gradient using water with 0.1% *v/v* formic acid as Phase A and acetonitrile with 0.1% *v/v* formic acid as Phase B. The separation started with an isocratic elution at 5% *v/v* B for 4 min, followed by a linear gradient from 5 to 10% *v/v* B over 4 min, from 10–15% *v/v* B over 5 min, from 15 to 100% *v/v* B over 2 min. The column was re-equilibrated with 5% *v/v* B for an additional 3 min. The injection volume was 5 µL and the flow rate was set to 0.5 mL min^{-1}. The drawing and ejection speed were set to 100 µL min^{-1} and 400 µL min^{-1}, respectively. The ESI source parameters were set as follows: product ion spectra were recorded in data-dependent acquisition (DDA) mode with a mass range from *m/z* 180 to *m/z* 2000 (MS1: FTMS, normal, resolution = 60,000, full, positive; MS2: FTMS, normal, resolution = 30,000, positive). An auxiliary gas flow of 10 units, capillary temperature of 270 °C, capillary voltage of 1 V, sheath gas flow of 45 units, and source voltage of 4000 V were used. The parameter for the DDA mode was set as follows: activation type: CID, minimum signal required: 10,000, isolation width: *m/z* 2.00, normalized collision energy: 35.0, default charge state: 2, activation Q: 0.250, and activation time: 30 ms. The dynamic exclusion enabled was set as follows: repeat count: 3, repeat duration: 30 s, exclusion list size: 50, and exclusion duration: 180 s. To analyze the pure compound (KmcB), the above gradient was optimized as it started isocratically with 5% *v/v* B for 4 min, followed by a linear gradient from 5 to 100% *v/v* B over 5 min. The column was re-equilibrated with 5% *v/v* B for an additional 3 min. The mass range was from *m/z* 500 to *m/z* 2000. For MS/MS fragmentation, the product ions were formed by in-source surface-induced dissociation (SID: 70 V). The mass range spanned from *m/z* 100 to *m/z* 2000. Alternatively, the two most intensive precursors per MS1 were selected for subsequent collision-induced dissociation (CID: 35 V). The MS and MS/MS data derived from the LTQ-Orbitrap XL were acquired with Xcalibur 2.2 (Thermo Fisher Scientific GmbH, Bremen, Germany), displayed and analyzed with Freestyle 1.8 SP2 (Thermo Fisher Scientific GmbH, Bremen, Germany).

D-Ala-D-Ala based affinity chromatography

Activation of 5 mL HiTrap NHS-activated HP affinity columns (GE Healthcare) and ligand binding was conducted as described before[90] with slight modifications. Briefly, the resin was activated with 30 mL of 1 mM HCl, followed by injection of 200 mM D-Ala-D-Ala dipeptide, dissolved into 5 mL of coupling buffer (0.2 M $NaHCO_3$, 0.5 M NaCl, pH 8.3). After 30 min incubation, the resin was washed with 0.5 M ethanolamine hydrochloride, 0.5 M NaCl (pH 8.3, 30 mL – Buffer A), followed by 0.1 M sodium acetate, 0.5 mM NaCl (pH 4.0, 30 mL – Buffer B), and again 30 mL of Buffer A. After 30 min incubation, the resin was washed with three cycles of Buffer B, Buffer A, and Buffer B. Culture extracts were prepared as described above and their pH brought back to 8.0 using HCl 6 N. They were then filtered with a cut-off of 0.22 µm and loaded onto D-Ala-D-Ala column at a flow rate of 0.5 mL min^{-1}. After extensive washing with coupling buffer, the bound GPA was eluted with 0.1 M ammonium hydroxide and the eluate was lyophilized to obtain a crude pre-fractionated GPA mixture.

Purification of KmcB

An Agilent 1100 system consisting of a G1312A binary pump, a G1315D diode array detector (DAD), a G1316A column compartment, a G1329A automatic liquid sampler (ALS) and a G1364C analytical fraction collector (FC) was used for KmcB purification. The analytical HPLC chromatograms were acquired and displayed with Agilent ChemStation for LC 3D systems B.03.02 (Agilent Technologies, Waldbronn, Germany). For purification, a partially purified crude extract (1.973 g) obtained by D-Ala-D-Ala based affinity chromatography was resuspended in MQ-H_2O to give a final concentration at 80 mg mL^{-1}, followed by centrifugation at 4000 rpm and 4 °C for 10 min (Eppendorf® Centrifuge 5810 R). The separation of the supernatant obtained was carried out using a Fortis Diphenyl column (150 × 4.6 mm, 5 µm, Fortis Technologies Ltd., Cheshire, UK), which was eluted by a linear gradient using water with 0.1% *v/v* formic acid as Phase A and methanol with 0.1% *v/v* formic acid as Phase B. The gradient was started with an isocratic elution with 5% *v/v* B for 2 min, followed by a linear gradient from 5–10% *v/v* B over 10 min, from 10–35% *v/v* B over 2 min. The column was washed with 100% *v/v* B for 1.5 min and re-equilibrated with 5% *v/v* B for an additional 4.5 min. The injection volume was 60 µL. The flow rate and UV monitoring were set to 1.0 mL min^{-1} and 236 nm, respectively. All fractions containing KmcB were pooled. 6.1 mg of pure KmcB was obtained after evaporation and lyophilization.

NMR spectroscopy

1D- and 2D-NMR spectra were acquired on a Bruker Avance III 700 MHz spectrometer (700 MHz for ^{1}H, and 176 MHz for ^{13}C) with a 5 mm TXI probe (Bruker, Karlsruhe, Germany) at 298 K. The ^{1}H and ^{13}C NMR chemical shifts were referenced to the solvent peaks at 2.50 ppm (^{1}H) and 39.5 ppm (^{13}C) for DMSO when DMSO-d_6 was utilized as solvent. TopSpin 3.5 (Bruker, Karlsruhe, Germany) was used for data acquisition and TopSpin 4.1.4 (Bruker, Karlsruhe, Germany) for data processing.

Advanced Marfey's amino analysis

KmcB (0.35 mg) was hydrolyzed with stirring in 6 N HCl (200 µL) at 110 °C for 12 h. The acid hydrolysates were frozen at −80 °C followed by lyophilization. The dry acid hydrolysates were resuspended in H_2O (50 µL; analytical grade) and equally divided into two portions A (25 µL) and B (25 µL). Portion A was treated with 1 M $NaHCO_3$ (10 µL) and then with Marfey's reagent L-FDLA (50 µL of a 10 mg mL^{-1} solution in acetone), and the mixture was stirred at 37 °C for 1 h. The reaction was quenched with 1 N HCl (10 µL) and diluted with MeOH (105 µL) up to a final volume of 200 µL. Portion B was treated following the similar protocol but with L-FDLA (25 µL of a 10 mg mL^{-1} solution in acetone) and D-FDLA (25 µL of a 10 mg mL^{-1} solution in acetone). Authentic standards of L-Ile, L-*allo*-Ile, and D-Ile were treated with L-FDLA and D/L-FDLA as described above and yielded the L-FDLA and D-FDLA derivatives of standards[91]. Sample analysis was carried out with the HPLC-ESI-HRMS mass spectrometer as described above but in negative ionization mode. The column was eluted isocratically at 5% *v/v* B for 5 min, followed by a linear gradient from 5–50% *v/v* B over 40 min, from 50–100% *v/v* B over 5 min. The column was re-equilibrated with 5% *v/v* B for an additional 5 min. The injection volume was 5 µL and the flow rate was set to 0.5 mL min^{-1}. The detection mass range was set between *m/z* 100 to *m/z* 1000.

Minimum Inhibitory Concentration (MIC) and Minimal Bactericidal Concentration (MBC) determination

MICs and MBCs of Kmc, vancomycin, and teicoplanin towards a panel of Gram-positive and Gram-negative bacteria were determined following the guidelines of the Clinical and Laboratory Standards Institute[83], with broth dilution method in Müller Hinton Broth, cation adjusted (MHB2). *Escherichia coli* ATCC 35218, *Moraxella catarrhalis* ATCC 3293, *Staphylococcus aureus* ATCC 6538 P (MSSA), *Staphylococcus aureus* ATCC 25923 (MSSA), *Staphylococcus aureus* ATCC 43300 (MRSA), *Enterococcus faecalis* ATCC 29212, and *Enterococcus faecalis* ATCC 51299 (VanB phenotype) were obtained from the American Type Culture Collection (ATCC). *Enterococcus faecalis* 9160188401-EF-34 (VanA phenotype) and *Staphylococcus epidermidis* strain 4 are clinical isolates, kindly provided by Laboratorio Microbiologia Clinica—Ospedale di Circolo, Varese, Italy.

Staphylococcus haemolyticus 3902 is a teicoplanin-resistant clinical isolate[104], received from FIIRV (Fondazione Istituto Insubrico Ricerca per la Vita), Gerenzano Varese, Italy. For long-term preservation, bacterial cultures were stored at −80 °C in 10% *v/v* glycerol.

For MIC determination, 50 µL of a suspension of bacterial cells in exponential growth phase (at 1 × 10^6 colony forming unit (CFU) mL^{-1} concentration) in MHB2 were inoculated in 96-well plates, together with 50 µL of GPA (from 0 to 128 µg mL^{-1} final concentration). Plates were then incubated for 20 h at 37 °C and 100 rpm. MICs were expressed as the minimal concentration of antibiotic at which no turbidity could be detected. For MBC determination, the content of the wells in which no growth was observed, was spread in 48-well plates containing 900 µL of Müller Hinton Agar, incubated at 37 °C for 24 h. MBCs were defined as the lowest concentration of antibiotic at which no growth could be seen. All experiments were repeated at least in triplicate.

Isolation of genomic DNA from *A. auranticolor* DSM 44650

Genomic DNA, further used as a positive control in semi-quantitative RT-PCR analysis, was isolated from *A. auranticolor* DSM 44650 using the Kirby procedure[78]. For the genome sequencing, genomic DNA of *A. auranticolor* DSM 44650 was extracted using the NucleoSpin® Microbial DNA kit (MACHEREY-NAGEL GmbH & Co. KG) according to the supplier's protocol.

RNA isolation from *A. auranticolor* DSM 44650, cDNA synthesis, and semi-quantitative RT-PCR

RNA was isolated from vegetative mycelium of *A. auranticolor* DSM 44650 obtained from three independent Kmc producing cultures cultivated for 96 h in R5 medium. RNAqueous Phenol-free total RNA isolation kit (Invitrogen, Thermo Fisher Scientific, Waltham, USA) was used for RNA isolation according to the protocol of supplier, but omitting the on-column DNase treatment step. Isolated RNA samples (contaminated with DNA) were further subjected to first DNase treatment (1 h at 37 °C), using 1 U of DNase I, RNase-free (Thermo Fisher Scientific, Waltham, USA) per 10 µL of solution. After first DNase treatment, RNA concentration and quality were assessed using DeNovix DS-11 FX+ (DeNovix Inc., Wilmington, USA), and 50 µg of RNA were subjected to a second DNase treatment with 8 U of DNase I, RNase-free (Thermo Fisher Scientific, Waltham, USA) for 2 h at 37 °C. To test if the second DNase treatment removed all residual DNA contamination, 1 µL of the mixture was used as a template for PCR with HrdB_Akin_F/R (Supplementary Table 10) to amplify the 253 bp internal region of *hrdB* (RNA polymerase sigma factor gene, *V5P93_005973*); in case the results of PCR were negative, DNAse was inactivated by adding 10% *v/v* EDTA (50 mM) and incubating it at 65 °C for 10 min, otherwise additional DNase treatment step was performed. Concentration and quality of DNA-free RNA sample was assessed using DeNovix DS-11 FX+ (DeNovix Inc., Wilmington, USA), and 5 µg of RNA were subjected to the cDNA synthesis step using RevertAid First Strand cDNA Synthesis Kit (Thermo Fisher Scientific, Waltham, USA) according to the supplier's protocol. 1 µL of cDNA obtained in the previous step was used as a template for the PCR reaction with Q5 High-Fidelity DNA Polymerase (New England Biolabs, Ipswich, USA) and oligonucleotide primers listed in Supplementary Table 10. This reaction was set in parallel with the positive control reaction (with 100 ng of gDNA as a template) and a negative control reaction (with 1 µL of DNA-free RNA sample). Obtained amplicons were visualized by horizontal 2% *w/v* agarose (Thermo Fisher Scientific, Waltham, USA) gel-electrophoresis using GeneRuler 1 kb DNA Ladder (Thermo Fisher Scientific, Waltham, USA).

Sequencing and complete assembly of *A. auranticolor* DSM 44650 genome

Long and short DNA reads were generated by Nanopore and Illumina sequencing, respectively. For library preparation, the TruSeq DNA PCR-free high-throughput library prep kit (Illumina) and the SQK-LSK112 sequencing kit (Oxford Nanopore Technologies [ONT]) were used without prior shearing of the DNA. To generate the short reads, a 2 × 300-nucleotide run (MiSeq reagent kit v3, 600 cycles) was executed. The long reads were generated on a GridION platform using a R9.4.1 flow cell. Base calling and demultiplexing were performed using GUPPY v6.3.8.0 with the super-accurate basecalling model. Assemblies were done using FLYE v.2.9[105] for the Nanopore long read data and NEWBLER v2.8[106] for the Illumina short read data. After polishing of the FLYE-based assembly using PILON v1.22[107] using BOWTIE2[108] for mapping, the respective FLYE and NEWBLER assemblies were combined in CONSED v28.0[109]. The resulting single contig representing the circular genome was annotated using the PGAP pipeline[110,111]. All raw sequencing data are available via BioProject ID PRJNA1076217. The annotated genome is accessible via GenBank ID CP154825.

Details of in silico analysis

MultiGeneBlast[56] was used to search annotated *Pseudonocardiales* spp. genomes, available in GenBank, for co-localized homologs of *bbr, oxyA, oxyB*, and *oxyC* from balhimycin BGC (Y16952.3) under the default parameters (except "maximum distance between genes in locus (kb)" parameter, that was set to 34 kbp – distance between *bbr* and *oxyC*). antiSMASH 7.0[57] was used for the automated annotation of GPA BGCs, prediction of the module/domain organization of NRPSs, and non-ribosomal codes. MEGA 11.0.13[112] package was used for the phylogenetic reconstructions. GENEIOUS 4.8.5[113] was used for the oligonucleotide primer design and routine analysis of nucleic acid and amino acid sequences.

Reporting summary

Further information on research design is available in the Nature Portfolio Reporting Summary linked to this article.

Data availability

All unique reagents generated in this study are available from the corresponding authors upon reasonable request. The availability of kineomicins may be limited to a small batch and might require preparation. The published article includes all biological data generated during this study. Complete genome assembly of *A. auranticolor* DSM 44650 was deposited to the GenBank under the CP154825 accession number. All mass spectrometry data, obtained in this work, were deposited in the MassIVE mass spectrometry data repository (MSV000097194 dataset).

Received: 15 January 2025; Accepted: 23 April 2025;
Published online: 03 May 2025

References

1. Nicolaou, K. C., Boddy, C. N. C., Bräse, S. & Winssinger, N. Chemistry, biology, and medicine of the glycopeptide antibiotics. *Angew. Chem. - Int. Ed.* **38**, 2096–2152 (1999).
2. Yushchuk, O. & Ostash, B. Glycopeptide antibiotics: genetics, chemistry, and new screening approaches. In *Natural Products from Actinomycetes* (eds. Rai, R. V. & Bai, J. A.) (Springer, 2022).
3. Yim, G., Thaker, M. N., Koteva, K. & Wright, G. Glycopeptide antibiotic biosynthesis. *J. Antibiot. (Tokyo).* **67**, 31–41 (2014).
4. Hansen, M. H., Stegmann, E. & Cryle, M. J. Beyond vancomycin: recent advances in the modification, reengineering, production and discovery of improved glycopeptide antibiotics to tackle multidrug-resistant bacteria. *Curr. Opin. Biotechnol.* **77**, 102767 (2022).
5. Van Bambeke, F. Lipoglycopeptide antibacterial agents in gram-positive infections: a comparative review. *Drugs* **75**, 2073–2095 (2015).
6. Van Bambeke, F. Glycopeptides in clinical development: pharmacological profile and clinical perspectives. *Curr. Opin. Pharmacol.* **4**, 471–478 (2004).
7. Xu, L. et al. Complete genome sequence and comparative genomic analyses of the vancomycin-producing *Amycolatopsis orientalis*. *BMC Genomics* **15**, 1–18 (2014).

8. Thaker, M. N. et al. Identifying producers of antibacterial compounds by screening for antibiotic resistance. *Nat. Biotechnol.* **31**, 922–927 (2013).
9. Bardone, M. R., Paternoster, M. & Coronelli, C. Teichomycins, new antibiotics from *Actinoplanes teichomyceticus* nov. sp. II. Extraction and chemical characterization. *J. Antibiot. (Tokyo).* **31**, 170–177 (1978).
10. Van Groesen, E., Innocenti, P. & Martin, N. I. Recent advances in the development of semisynthetic glycopeptide antibiotics: 2014-2022. *ACS Infect. Dis.* **8**, 1381–1407 (2022).
11. Goldstein, B. P. et al. A40926, a new glycopeptide antibiotic with anti-*Neisseria* activity. *Antimicrob. Agents Chemother.* **31**, 1961–1966 (1987).
12. Hamill, R. L., Mabe, J. A., Mahoney, D. F., Nakatsukasa, W. M., Yao, R. C. *A82846 antibiotics (U. S. Patent No. US5312738A). U.S. Patent and Trademark Office.* https://patents.google.com/patent/US5312738A/en. (1987)
13. Levine, D. P. Vancomycin: a history. *Clin. Infect. Dis.* **42**, S5–S12 (2006).
14. Levine, J. F. Vancomycin: a review. *Med. Clin. North Am.* **71**, 1135–1145 (1987).
15. Grundy, W. E. et al. Ristocetin, microbiologic properties. *Antibiot. Annu*. **1956**, 687–692 (1956).
16. Cavalleri, B., Pagani, H., Volpe, G., Selva, E. & Parenti, F. A-16686, a new antibiotic from *Actinoplanes*: I. Fermentation, isolation and preliminary physico-chemical characteristics. *J. Antibiot. (Tokyo).* **37**, 309–317 (1984).
17. Williams, D. H. The glycopeptide story – how to kill the deadly 'superbugs. *Nat. Prod. Rep.* **13**, 469–477 (1996).
18. Parenti, F. & Cavalleri, B. Proposal to name the vancomycin-ristocetin like glycopeptides as dalbaheptides. *J. Antibiot. (Tokyo).* **42**, 1882–1883 (1989).
19. Stegmann, E. et al. Genetic analysis of the balhimycin (vancomycin-type) oxygenase genes. *J. Biotechnol.* **124**, 640–653 (2006).
20. Xu, F. et al. A genetics-free method for high-throughput discovery of cryptic microbial metabolites. *Nat. Chem. Biol.* **15**, 161–168 (2019).
21. Spohn, M. et al. Overproduction of ristomycin a by activation of a silent gene cluster in *Amycolatopsis japonicum* MG417-CF17. *Antimicrob. Agents Chemother.* **58**, 6185–6196 (2014).
22. Yushchuk, O., Ostash, B., Truman, A. W., Marinelli, F. & Fedorenko, V. Teicoplanin biosynthesis: unraveling the interplay of structural, regulatory, and resistance genes. *Appl. Microbiol. Biotechnol.* **104**, 3279–3291 (2020).
23. Greule, A. et al. Kistamicin biosynthesis reveals the biosynthetic requirements for production of highly crosslinked glycopeptide antibiotics. *Nat. Commun*. **10**, 2613 (2019).
24. van Wageningen, A. M. et al. Sequencing and analysis of genes involved in the biosynthesis a vancomycin group antibiotic. *Chem. Biol.* **5**, 155–162 (1998).
25. Chiu, H. T. et al. Molecular cloning and sequence analysis of the complestatin biosynthetic gene cluster. *Proc. Natl Acad. Sci. USA.* **98**, 8548–8553 (2001).
26. Li, T. L. et al. Biosynthetic gene cluster of the glycopeptide antibiotic teicoplanin: characterization of two glycosyltransferases and the key acyltransferase. *Chem. Biol.* **11**, 107–119 (2004).
27. Sosio, M., Stinchi, S., Beltrametti, F., Lazzarini, A. & Donadio, S. The gene cluster for the biosynthesis of the glycopeptide antibiotic A40926 by *Nonomuraea* species. *Chem. Biol.* **10**, 541–549 (2003).
28. Recktenwald, J. et al. Nonribosomal biosynthesis of vancomycin-type antibiotics: a heptapeptide backbone and eight peptide synthetase modules. *Microbiology* **148**, 1105–1118 (2002).
29. Woithe, K. et al. Oxidative phenol coupling reactions catalyzed by OxyB: a cytochrome P450 from the vancomycin producing organism. Implications for vancomycin biosynthesis. *J. Am. Chem. Soc.* **129**, 6887–6895 (2007).
30. Hubbard, B. K. & Walsh, C. T. Vancomycin assembly: nature's way. *Angew. Chem. Int. Ed. Engl.* **42**, 730–765 (2003).
31. Sandercock, A. M. et al. Biosynthesis of the di-meta-hydroxyphenylglycine constituent of the vancomycin-group antibiotic chloroeremomycin. *Chem. Commun*. **2001**, 1252–1253 (2001)
32. Pfeifer, V. et al. A polyketide synthase in glycopeptide biosynthesis. The biosynthesis of the non-proteinogenic amino acid (S)-3,5-dihydroxyphenylglycine. *J. Biol. Chem.* **276**, 38370–38377 (2001).
33. Puk, O. et al. Biosynthesis of chloro-β-hydroxytyrosine, a nonproteinogenic amino acid of the peptidic backbone of glycopeptide antibiotics. *J. Bacteriol.* **186**, 6093–6100 (2004).
34. Kirkpatrick, P. N. et al. Characterisation of a sugar epimerase enzyme involved in the biosynthesis of a vancomycin-group antibiotic. *Chem. Commun.* **17**, 1565–1566 (2000).
35. Pelzer, S. et al. Identification and analysis of the balhimycin biosynthetic gene cluster and its use for manipulating glycopeptide biosynthesis in *Amycolatopsis mediterranei* DSM5908. *Antimicrob. Agents Chemother.* **43**, 1565–1573 (1999).
36. Losey, H. C. et al. Tandem action of glycosyltransferases in the maturation of vancomycin and teicoplanin aglycones: тovel glycopeptides. *Biochemistry* **40**, 4745–4755 (2001).
37. Losey, H. C. et al. Incorporation of glucose analogs by GtfE and GtfD from the vancomycin biosynthetic pathway to generate variant glycopeptides. *Chem. Biol.* **9**, 1305–1314 (2002).
38. Yim, G. et al. Harnessing the synthetic capabilities of glycopeptide antibiotic tailoring enzymes: characterization of the UK-68,597 biosynthetic cluster. *ChemBioChem*. **15**, 2613–2623 (2014).
39. Truman, A. W. et al. Antibiotic resistance mechanisms inform discovery: identification and characterization of a novel *Amycolatopsis* strain producing ristocetin. *Antimicrob. Agents Chemother.* **58**, 5687–5695 (2014).
40. Xu, M. et al. GPAHex – a synthetic biology platform for type IV–V glycopeptide antibiotic production and discovery. *Nat. Commun*. **11**, 5232 (2020).
41. Waglechner, N., McArthur, A. G. & Wright, G. D. Phylogenetic reconciliation reveals the natural history of glycopeptide antibiotic biosynthesis and resistance. *Nat. Microbiol.* **4**, 1862–1871 (2019).
42. Culp, E. J. et al. Evolution-guided discovery of antibiotics that inhibit peptidoglycan remodelling. *Nature* **578**, 582–587 (2020).
43. Xu, M. et al. Phylogeny-informed synthetic biology reveals unprecedented structural novelty in type V glycopeptide antibiotics. *ACS Cent. Sci.* **8**, 615–626 (2022).
44. Hansen, M. H. et al. Resurrecting ancestral antibiotics: unveiling the origins of modern lipid II targeting glycopeptides. *Nat. Commun.* **14**, 7842 (2023).
45. Yue, X., Xia, T., Wang, S., Dong, H. & Li, Y. Highly efficient genome editing in *N. gerenzanensis* using an inducible CRISPR/Cas9–RecA system. *Biotechnol. Lett.* **42**, 1699–1706 (2020).
46. Yushchuk, O. et al. New molecular tools for regulation and improvement of A40926 glycopeptide antibiotic production in *Nonomuraea gerenzanensis* ATCC 39727. *Front. Microbiol*. https://doi.org/10.3389/fmicb.2020.00008 (2020).
47. Haslinger, K., Peschke, M., Brieke, C., Maximowitsch, E. & Cryle, M. J. X-domain of peptide synthetases recruits oxygenases crucial for glycopeptide biosynthesis. *Nature* **521**, 105–109 (2015).
48. Peschke, M., Haslinger, K., Brieke, C., Reinstein, J. & Cryle, M. J. Regulation of the P450 oxygenation cascade involved in glycopeptide antibiotic biosynthesis. *J. Am. Chem. Soc.* **138**, 6746–6753 (2016).
49. Schoppet, M., Tailhades, J., Kulkarni, K. & Cryle, M. J. Precursor manipulation in glycopeptide antibiotic biosynthesis: are β-amino acids compatible with the oxidative cyclization cascade? *J. Org. Chem.* **83**, 7206–7214 (2018).

50. Gavriilidou, A. et al. Phylogenetic distance and structural diversity directing a reclassification of glycopeptide antibiotics. *bioRxiv* https://doi.org/10.1101/2023.02.10.526856 (2023)
51. Nouioui, I. et al. Genome-based taxonomic classification of the phylum actinobacteria. *Front. Microbiol.* **9**, 1–119 (2018).
52. Andreo-Vidal, A., Binda, E., Fedorenko, V., Marinelli, F. & Yushchuk, O. Genomic insights into the distribution and phylogeny of glycopeptide resistance determinants within the *Actinobacteria* phylum. *Antibiotics* **10**, 1533 (2021).
53. Kunstmann, M. P., Mitscher, L. A., Porter, J. N., Shay, A. J. & Darken, M. A. LL-AV290, a new antibiotic. I. Fermentation, isolation, and characterization. *Antimicrob. Agents Chemother.* **8**, 242–245 (1968).
54. Liu, K. et al. Enhancing ristomycin a production by overexpression of ParB-like StrR family regulators controlling the biosynthesis genes. *Appl. Environ. Microbiol.* **87**, 1–19 (2021).
55. Adamek, M. et al. Comparative genomics reveals phylogenetic distribution patterns of secondary metabolites in *Amycolatopsis* species. *BMC Genomics* **19**, 426 (2018).
56. Medema, M. H., Takano, E. & Breitling, R. Detecting sequence homology at the gene cluster level with MultiGeneBLAST. *Mol. Biol. Evol.* **30**, 1218–1223 (2013).
57. Blin, K. et al. AntiSMASH 7.0: new and improved predictions for detection, regulation, chemical structures and visualisation. *Nucleic Acids Res.* **51**, W46–W50 (2023).
58. Menges, R., Muth, G., Wohlleben, W. & Stegmann, E. The ABC transporter Tba of *Amycolatopsis balhimycina* is required for efficient export of the glycopeptide antibiotic balhimycin. *Appl. Microbiol. Biotechnol.* **77**, 125–134 (2007).
59. Mulyani, S. et al. The thioesterase Bhp is involved in the formation of β-hydroxytyrosine during balhimycin biosynthesis in *Amycolatopsis balhimycina*. *ChemBioChem*. **11**, 266–271 (2010).
60. Stegmann, E., Frasch, H. J. & Wohlleben, W. Glycopeptide biosynthesis in the context of basic cellular functions. *Curr. Opin. Microbiol.* **13**, 595–602 (2010).
61. Omura, S. et al. Studies on bacterial cell wall inhibitors: VII. Azureomycins A and B, new antibiotics produced by *Pseudonocardia azurea* nov. sp. Taxonomy of the producing organism, isolation, characterization and biological properties. *J. Antibiot. (Tokyo).* **32**, 985–994 (1979).
62. Kaur, N., Kumar, S., Bala, M., Raghava, G. P. S. & Mayilraj, S. Draft genome sequence of *Amycolatopsis decaplanina* strain DSM 44594^T. *Genome Announc* **1**, e0013813 (2013).
63. Jørgensen, T. S. et al. Complete genome sequence of the rare actinobacterium *Kutzneria* sp. strain CA-103260. *Microbiol. Resour. Announc.* **10**, e0049921 (2021).
64. Stepanyshyn, A. et al. Complete genome assembly of *Amycolatopsis bartoniae* DSM 45807^T allows the characterization of a novel glycopeptide biosynthetic gene cluster. **15**, 1651 (2024).
65. Fujimori, D. G. et al. Cloning and characterization of the biosynthetic gene cluster for kutznerides. *Proc. Natl Acad. Sci. USA* **104**, 16498–16503 (2007).
66. Gao, W. et al. Discovery and characterization of the tuberculosis drug lead ecumicin. *Org. Lett.* **16**, 6044–6047 (2014).
67. Otoguro, M. et al. Numerical phenetic and phylogenetic analyses of *Actinokineospora* isolates, with a description of *Actinokineospora auranticolor* sp. nov. and *Actinokineospora enzanensis* sp. nov. *Actinomycetologica* **15**, 30–39 (2001).
68. Mascher, T., Zimmer, S. L., Smith, T. A. & Helmann, J. D. Antibiotic-inducible promoter regulated by the cell envelope stress-sensing two-component system LiaRS of *Bacillus subtilis*. *Antimicrob. Agents Chemother.* **48**, 2888–2896 (2004).
69. Mascher, T., Margulis, N. G., Wang, T., Ye, R. W. & Helmann, J. D. Cell wall stress responses in *Bacillus subtilis*: the regulatory network of the bacitracin stimulon. *Mol. Microbiol.* **50**, 1591–1604 (2003).
70. Andreo-Vidal, A., Yushchuk, O., Marinelli, F. & Binda, E. Cross-talking of pathway-specific regulators in glycopeptide antibiotics (teicoplanin and A40926) production. *Antibiotics* **12**, 641 (2023).
71. Marcone, G. L., Binda, E., Carrano, L., Bibb, M. & Marinelli, F. Relationship between glycopeptide production and resistance in the actinomycete *Nonomuraea* sp. ATCC 39727. *Antimicrob. Agents Chemother.* **58**, 5191–5201 (2014).
72. Taurino, C., Frattini, L., Marcone, G. L., Gastaldo, L. & Marinelli, F. *Actinoplanes teichomyceticus* ATCC 31121 as a cell factory for producing teicoplanin. *Microb. Cell Fact*. **10**, 82 (2011).
73. Su, W. & Beuchat, L. R. Combined effect of growth medium, age of cells and phase of sporulation on heat resistance and recovery of *Hansenula anomala*. *Mycopathologia* **87**, 129–134 (1984).
74. Shirling, E. B. & Gottlieb, D. Method for characterization of *Streptomyces* species. *Int. J. Syst. Bacteriol.* **16**, 313–340 (1966).
75. Koshla, O. et al. Gene *miaA* for post-transcriptional modification of $tRNA_{XXA}$ is important for morphological and metabolic differentiation in *Streptomyces*. *Mol. Microbiol.* **112**, 249–265 (2019).
76. Zahoor, T., Siddique, F. & Farooq, U. Isolation and characterization of vinegar culture (*Acetobacter aceti*) from indigenous sources. *Br. Food J.* **108**, 429–439 (2006).
77. Rebets, Y. et al. Production of landomycins in *Streptomyces globisporus* 1912 and *S. cyanogenus* S136 is regulated by genes encoding putative transcriptional activators. *FEMS Microbiol. Lett.* **222**, 149–153 (2003).
78. Kieser, T., Bibb, M. J., Buttner, M. J., Chater, K. F. & Hopwood, D. A. *Practical Streptomyces Genetics* (John Innes Foundation, 2000).
79. Neu, J. M. & Wright, G. D. Inhibition of sporulation, glycopeptide antibiotic production and resistance in *Streptomyces toyocaensis* NRRL 15009 by protein kinase inhibitors. *FEMS Microbiol. Lett.* **199**, 15–20 (2001).
80. Puk, O. et al. Glycopeptide biosynthesis in *Amycolatopsis mediterranei* DSM5908: function of a halogenase and a haloperoxidase/perhydrolase. *Chem. Biol.* **9**, 225–235 (2002).
81. Schäberle, T. F. et al. Self-resistance and cell wall composition in the glycopeptide producer *Amycolatopsis balhimycina*. *Antimicrob. Agents Chemother.* **55**, 4283–4289 (2011).
82. Yushchuk, O., Binda, E. & Marinelli, F. Glycopeptide antibiotic resistance genes: distribution and function in the producer actinomycetes. *Front. Microbiol*. https://doi.org/10.3389/fmicb.2020.01173 (2020).
83. Wayne, P. *Performance Standards for Antimicrobial Susceptibility Testing; Twenty-Third Informational Supplement. CLSI Document M100-S23. Performance Standards for Antimicrobial Susceptibility Testing.* https://clsi.org/shop/standards/m100/ (2013).
84. Thykaer, J. et al. Increased glycopeptide production after overexpression of shikimate pathway genes being part of the balhimycin biosynthetic gene cluster. *Metab. Eng.* **12**, 455–461 (2010).
85. Nadkarni, S. R. et al. Balhimycin, a new glycopeptide antibiotic produced by *Amycolatopsis* sp. Y-86,21022. Taxonomy, production, isolation and biological activity. *J. Antibiot. (Tokyo).* **47**, 334–341 (1994).
86. Goldfinger, V. et al. Metabolic engineering of the shikimate pathway in *Amycolatopsis* strains for optimized glycopeptide antibiotic production. *Metab. Eng.* **78**, 84–92 (2023).
87. Jung, H. M., Kim, S. Y., Moon, H. J., Oh, D. K. & Lee, J. K. Optimization of culture conditions and scale-up to pilot and plant

scales for vancomycin production by *Amycolatopsis orientalis*. *Appl. Microbiol. Biotechnol.* **77**, 789–795 (2007).
88. Horbal, L. et al. The pathway-specific regulatory genes, *tei15** and *tei16**, are the master switches of teicoplanin production in *Actinoplanes teichomyceticus*. *Appl. Microbiol. Biotechnol.* **98**, 9295–9309 (2014).
89. Ramoni, G. et al. New avoparcin-like molecules from the avoparcin producer *Amycolatopsis coloradensis* ATCC 53629. *Fermentation* **8**, 1–11 (2022).
90. Yushchuk, O. et al. Genomic-led discovery of a novel glycopeptide antibiotic by *Nonomuraea coxensis* DSM 45129. *ACS Chem. Biol.* **16**, 915–928 (2021).
91. Wu, Y. et al. Fuscasins A-D, cycloheptapeptides from the marine sponge *Phakellia fusca*. *J. Nat. Prod.* **82**, 970–979 (2019).
92. Jonker, H. R. A. et al. NMR spectroscopic characterization of the *C*-mannose conformation in a thrombospondin repeat using a selective labeling approach. *Angew. Chem. Int. Ed. Engl.* **59**, 20659–20665 (2020).
93. Deslauriers, R., Jarrell, H. C., Byrd, R. A. & Smith, I. C. Observation by ^{13}C NMR of metabolites in differentiating amoeba. Trehalose storage in encysted *Acanthamoeba castellanii*. *FEBS Lett.* **118**, 185–190 (1980).
94. Gerhard, U., Mackay, J. P., Maplestone, R. A. & Williams, D. H. The role of the sugar and chlorine substituents in the dimerization of vancomycin antibiotics. *J. Am. Chem. Soc.* **115**, 232–237 (1993).
95. Shawky, R. M. et al. The border sequence of the balhimycin biosynthesis gene cluster from *Amycolatopsis balhimycina* contains *bbr*, encoding a StrR-like pathway-specific regulator. *J. Mol. Microbiol. Biotechnol.* **13**, 76–88 (2007).
96. Lu, S. et al. CDD/SPARCLE: The conserved domain database in 2020. *Nucleic Acids Res*. **48**, D265–D268 (2020).
97. Drula, E. et al. The carbohydrate-active enzyme database: functions and literature. *Nucleic Acids Res*. **50**, D571–D577 (2022).
98. Yushchuk, O., Binda, E., Fedorenko, V. & Marinelli, F. Occurrence of *vanHAX* and related genes beyond the *Actinobacteria* phylum. *Genes (Basel)*. **13**, 1960 (2022).
99. Debono, M. et al. Actaplanin, new glycopeptide antibiotics produced by *Actinoplanes missouriensis* the isolation and preliminary chemical characterization of actaplanin. *J. Antibiot. (Tokyo).* **37**, 85–95 (1984).
100. Yushchuk, O. et al. Characterization of the post-assembly line tailoring processes in teicoplanin biosynthesis. *ACS Chem. Biol.* **11**, 2254–2264 (2016).
101. Alt, S. et al. Toward single-peak dalbavancin analogs through biology and chemistry. *ACS Chem. Biol.* **14**, 356–360 (2019).
102. Sosio, M., Canavesi, A., Stinchi, S. & Donadio, S. Improved production of A40926 by *Nonomuraea* sp. through deletion of a pathway-specific acetyltransferase. *Appl. Microbiol. Biotechnol.* **87**, 1633–1638 (2010).
103. James, R. C., Pierce, J. G., Okano, A., Xie, J. & Boger, D. L. Redesign of glycopeptide antibiotics: back to the future. *ACS Chem. Biol.* **7**, 797–804 (2012).
104. Beltrametti, F., Lazzarini, A., Brunati, C., Selva, E. & Marinelli, F. Production of demannosyl-A40926 by a *Nonomuraea* sp. ATCC 39727 mutant strain. *J. Antibiot. (Tokyo).* **56**, 310–313 (2003).
105. Kolmogorov, M., Yuan, J., Lin, Y. & Pevzner, P. A. Assembly of long, error-prone reads using repeat graphs. *Nat. Biotechnol.* **37**, 540–546 (2019).
106. Miller, J. R., Koren, S. & Sutton, G. Assembly algorithms for next-generation sequencing data. *Genomics* **95**, 315–327 (2010).
107. Walker, B. J. et al. Pilon: an integrated tool for comprehensive microbial variant detection and genome assembly improvement. *PLoS ONE* **9**, e112963 (2014).
108. Langmead, B. & Salzberg, S. L. Fast gapped-read alignment with Bowtie 2. *Nat. Methods* **9**, 357–359 (2012).
109. Gordon, D. & Green, P. Consed: A graphical editor for next-generation sequencing. *Bioinformatics* **29**, 2936–2937 (2013).
110. Li, W. et al. RefSeq: expanding the prokaryotic genome annotation pipeline reach with protein family model curation. *Nucleic Acids Res.* **49**, D1020–D1028 (2021).
111. Tatusova, T. et al. NCBI prokaryotic genome annotation pipeline. *Nucleic Acids Res.* **44**, 6614–6624 (2016).
112. Tamura, K., Stecher, G. & Kumar, S. MEGA11: molecular evolutionary genetics analysis version 11. *Mol. Biol. Evol.* **38**, 3022–3027 (2021).
113. Kearse, M. et al. Geneious basic: an integrated and extendable desktop software platform for the organization and analysis of sequence data. *Bioinformatics* **28**, 1647–1649 (2012).

Acknowledgements

This work was supported by Humboldt Research Fellowship for Postdocs from Alexander von Humboldt Foundation and Ministry of Education and Science of Ukraine BG-14E grant (to O.Y.); by Fondo per il Programma Nazionale di Ricerca e Progetti di Rilevante Interesse Nazionale (PRIN) for the project DiGlycAn—project number 2022J7W7LW (to F.B. and F.M.); by the University of Insubria grant Fondo di Ateneo per la Ricerca 2022 and 2023 (to F.M. and F.B.); by the University of Insubria Starting grant for young researchers 2022 and 2023 (to F.B.); and by the Deutsche Forschungsgemeinschaft—RTG 2473 'Bioactive Peptides', project number 392923329 (to L.Z. and R.D.S.). We would like to thank Dr. Elisa Binda from University of Insubria for her help with fermentation at bioreactor scale, and Dr. Enrico Selva for the enthusiastic support and the invaluable suggestions for kineomicins purification. O.Y. would like to thank all defenders of Ukraine, who made working on this manuscript possible. L.Z. gratefully acknowledges the China Scholarship Council (CSC) for a granted Ph.D. scholarship. L.B. is a Ph.D. student of the "Life Sciences and Biotechnology" course at University of Insubria.

Author contributions

O.Y., F.M., and R.D.S.—conceptualization; O.Y., F.B., L.Z., E.B., and L.B.—investigation; C.R.-R., T.B., and J.K.—software; O.Y., L.Z., C.R.-R.—formal analysis; F.B., L.Z., and R.D.S.—methodology; O.Y., F.B., L.Z., F.M., and R.D.S.—writing, original draft; F.M. and R.D.S.—supervision and funding acquisition.

Competing interests

The authors declare no competing interests.

Additional information

Supplementary information The online version contains supplementary material available at https://doi.org/10.1038/s42004-025-01534-x.

Correspondence and requests for materials should be addressed to Roderich D. Süssmuth or Flavia Marinelli.

Peer review information *Communications Chemistry* thanks Max Cryle and the other, anonymous, reviewers for their contribution to the peer review of this work. Peer review reports are available.